Evidence for Autotrophic Growth of Purple Sulfur Bacteria using Pyrite as Electron and Sulfur Source

Hugo V. Alarcon[1], Jonathon E. Mohl[2,3], Grace W. Chong[4], Ana Betancourt[3], Yi Wang[5], Weinan Leng[6], Jason C. White[5], Jie Xu[1,4,7,*]

[1]Environmental Science and Engineering Program, the University of Texas at El Paso, El Paso, TX, USA

[2]Department of Mathematical Sciences, the University of Texas at El Paso, El Paso, TX, USA

[3]Border Biomedical Research Center, the University of Texas at El Paso, El Paso, TX, USA

[4]Department of Earth, Environmental and Resource Sciences, the University of Texas at El Paso, El Paso, TX, USA

[5]The Connecticut Agricultural Experiment Station, New Haven, CT, USA

[6]The National Center for Earth and Environmental Nanotechnology Infrastructure, Blacksburg, VA, USA

[7]School of Molecular Sciences, Arizona State University, Tempe, AZ, USA

*Correspondence should be sent to: jie.xu.gail@asu.edu

Abstract

Purple sulfur bacteria (PSB) are capable of anoxygenic photosynthesis via oxidizing reduced sulfur compounds and are considered key drivers of the sulfur cycle in a range of anoxic environments. In this study, we show that *Allochromatium vinosum* (a PSB species) is capable of autotrophic growth using pyrite as the electron and sulfur source. Comparative growth profile, substrate characterization, and transcriptomic sequencing data provided valuable insight into the molecular mechanisms underlying the bacterial utilization of pyrite and autotrophic growth. Specifically, the pyrite-supported cell cultures ("py"') demonstrated robust but much slower growth rates and distinct patterns from their sodium sulfide-amended positive controls. Up to ~ 200-fold upregulation of genes encoding various *c*- and *b*-type cytochromes was observed in

26 “py”, pointing to the high relevance of these molecules in scavenging and relaying electrons
27 from pyrite to cytoplasmic metabolisms. Conversely, extensive downregulation of genes related
28 to LH and RC complex components indicates that the electron source may have direct control
29 over the bacterial cells’ photosynthetic activity. In terms of sulfur metabolism, genes encoding
30 periplasmic or membrane-bound proteins (e.g., FccAB and SoxYZ) were largely upregulated
31 whereas those encoding cytoplasmic proteins (e.g., Dsr and Apr groups) are extensively
32 suppressed. Other notable differentially expressed genes are related to flagella/fimbriae/pilin(+),
33 metal efflux(+), ferrienterochelin(-), and [NiFe] hydrogenases(+). Characterization of the
34 biologically reacted pyrite indicates the presence of polymeric sulfur. These results have, for the
35 first time, put the interplay of PSB and transition metal sulfide chemistry under the spotlight,
36 with the potential to advance multiple fields, including metal and sulfur biogeochemistry,
37 bacterial extracellular electron transfer, and artificial photosynthesis.
38

39 ## Importance

40 Microbial utilization of solid-phase substrates constitutes a critical area of focus in
41 environmental microbiology, offering valuable insights into microbial metabolic processes and
42 adaptability. Recent advancements in this field have profoundly deepened our knowledge of
43 microbial physiology pertinent to these scenarios and spurred innovations in biosynthesis and
44 energy production. Furthermore, research into interactions between microbes and solid-phase
45 substrates has directly linked microbial activities to the surrounding mineralogical environments,
46 thereby enhancing our understanding of the relevant biogeochemical cycles. Our study represents
47 a significant step forward in this field by demonstrating, for the first time, the autotrophic growth
48 of purple sulfur bacteria using insoluble pyrite (FeS_2) as both the electron and sulfur source. The

presented comparative growth profiles, substrate characterizations, and transcriptomic sequencing data shed light on the potential relationships among electron donor types, photosynthetic reaction center activities, and potential extracellular electron transfer in these organisms capable of anoxygenic photosynthesis. Furthermore, the findings of our study may provide new insights into early-Earth biogeochemical evolutions, offering valuable constraints for understanding the environmental conditions and microbial processes that shaped our planet's history.

Keywords

purple sulfur bacteria, pyrite, anoxygenic photosynthesis, transcriptomic sequencing, cytochrome, iron sulfur cluster, *Allochromatium vinosum*

Introduction

Purple bacteria are photosynthetic, Gram-negative prokaryotes that convert light energy into chemical energy through the process of anoxygenic photosynthesis[1]. Anoxic conditions are required for purple bacteria to grow phototrophically, as the biosynthesis of their pigments and complexes is repressed by molecular oxygen[2]. While purple bacteria can utilize a wide range of electron donors to couple their autotrophic CO_2 fixation, a subgroup preferentially oxidize reduced sulfur compounds (i.e., hydrogen sulfide) during their phototrophic growth and are named purple sulfur bacteria (PSB). Almost all identified PSB belong to *Chromatiaceae*, *Ectothiorhodospiraceae* or *Halorhodospiraceae* families[3]. A key difference between these families of PSB lies in the location of the sulfur globules formed during the bacterial growth on reduced sulfur[4], which occur intracellularly in members of *Chromatiaceae* but extracellularly in

those of *Ectothiorhodospiraceae/ Halorhodospiraceae*. The specific strain studied in this reported work, *Allochromatium vinosum* DSM180, belongs to *Chromatiaceae*. Purple sulfur bacteria can thrive in various freshwater, marine and hypersaline environments that contain hydrogen sulfide and are illuminated, usually inhabiting the stratum below oxygenic phototrophs. A consequence of this is that the wavelengths of light reaching purple sulfur (and non-sulfur) bacteria are limited, due to the absorption of the blue and red regions in the solar spectrum by the chlorophyll-containing oxygenic phototrophs[5]. The most essential pigments in PSB are capable of absorbing near infrared and green light and use it for anoxygenic photosynthesis. PSB are key participants in the anoxic cycling of carbon, mostly as primary producers fixing CO_2 and occasionally as light-stimulated consumers of reduced organic compounds[6-9]. The most critical roles of PSB in ecosystems, however, lies in their capability of reoxidizing hydrogen sulfide produced by sulfate-reducers[1]. Hydrogen sulfide is a highly poisonous substance for most biota. The reoxidation of sulfide by PSB yields nontoxic forms of sulfur, such as elemental sulfur (S^0) and sulfate (SO_4^{2-}), thereby detoxifying the associated environments and importantly, closing the essential sulfur oxidation-reduction cycle.

Photosynthetic pathways in phototrophic purple bacteria (including PSB) have been studied for decades[10-17]. Here, we will briefly describe the phototrophic pathway in PSB. In PSB, incident photons are absorbed by an array of light-harvesting (LH) complexes within the intracytoplasmic membrane. These complexes consist of proteins that contain bacteriochlorophyll (BChl) and carotenoid pigments, which can absorb light energy through transforming their bonding and electronic states and funnel it down an energy gradient to a central reaction center (RC). In RC, charge separation occurs across the membrane and drives a series of redox reactions involving other biomolecules or protein complexes such as

95 quinone/quinol, cytochrome *b/c*, and cytochrome *c* complexes bound within the membrane.
96 Along with the electron transport, proton motive force (PMF) is formed and powers ATP
97 synthase complexes. Weissgerber *et al.*[18] sequenced and annotated the full genome of *A.*
98 *vinosum,* identifying three subunits of the RC, *pufC*, *pufM* and *pufL,* which are clustered and co-
99 transcribed with three sets of *pufA* and *pufB* genes encoding light-harvesting complex (LH1)
100 apoproteins[19]. Six potential *puc* gene pairs were also identified that encode α- and β- apoproteins
101 for several LH2 complex types[20]. It was reported that *A. vinosum* produces one type of
102 bacteriochlorophyll, namely BChl*a*, and carotenoids of the spirilloxanthin series[18].

103 A central feature of PSB is their capability to oxidize reduced sulfur compounds during
104 photolithoautotrophic growth. The known substrates that can be used by PSB include sulfide,
105 polysulfides, elemental sulfur, and thiosulfate[21]. In terms of sulfide oxidation, *A. vinosum* has the
106 genetic capacity to form several different enzymes, including the periplasmic flavocytochrome *c*
107 sulfide dehydrogenase (Fcc), and membrane-bound sulfide:quinone-oxidoreductases (Sqr),
108 which are predicted to be oriented toward the periplasm[22,23]. *A. vinosum* was also shown to
109 contain the genetic information for rhodaneses, sulfur relay proteins, and polysulfide reductase-
110 like proteins with unknown functions[24-27]. Some PSB including *A. vinosum* have been shown to
111 oxidize externally supplied elemental sulfur[28]. However, controversy exists regarding if PSB
112 may utilize commercially available elemental sulfur and it remains unknown how PSB may bind,
113 activate, and take up solid-phase sulfur. In principle, bacterial cells may interact with their
114 insoluble substrate through direct physical contact via outer membrane proteins or through
115 excreting extracellular substances that solubilize the substrate. For *A. vinosum*, evidence for the
116 formation of soluble intermediates like sulfide or polysulfides during uptake of elemental sulfur
117 was not obtained[29], rendering direct cell-sulfur contact as a likely option for the cells' interaction

118 with the solid substrate. It was also shown that *A. vinosum* strongly prefers the polymeric sulfur
119 fraction (i.e., sulfur chains) of the elemental sulfur and is likely unable to utilize the S_8 rings[30].
120 Regarding sulfur-oxidation in *A. vinosum*, many of the former studies have also focused on the
121 mechanisms involved in their sulfur globule utilization and proposed that the dissimilatory sulfite
122 reductase (Dsr) system might play essential roles as several *dsr*-deleted mutants of *A. vinosum*
123 were found unable to degrade these globules[31-34].

124 It remains unknown if *A. vinosum* or other PSB are capable of utilizing other solid-phase
125 substrates besides elemental sulfur. In the various habitats of PSB through geological time, there
126 had been, and still are, high chances of metal sulfide formation, which may divert free sulfide out
127 of the sulfur cycle and complicate the associated metal-sulfur geochemistry (**Fig. 1**). Interaction
128 of PSB with metal sulfides in general therefore may have its evolutionary basis, especially
129 considering the prevalence and transformations of sulfide-dominated environments on early
130 Earth. Based on previous studies[35,36], the oceans during the Mesoproterozoic Era were overall
131 constrained to support a mix of sulfidic, ferruginous, and oxic conditions. Later statistical
132 treatment of the available iron speciation data suggests that euxinic conditions were relatively
133 common[37,38], which may have provided a strong sink for Fe(II), leading to extensive FeS
134 formation. For modern geochemical settings, partial documentation of coexistence of Fe sulfide
135 precipitates and microbial sulfide oxidation (including phototrophic) was available for euxinic or
136 ferruginous lakes[39-41], fjords[42-44], estuaries[45-47], and shallow marine basins[48-50]. Iron monosulfide
137 in geochemical setting is a metastable phase and will eventually transform into greigite and
138 pyrite[51-55].

139 Here, we present the first evidence for *A. vinosum*'s capability of utilizing solid-phase
140 metal sulfide, i.e., pyrite (FeS_2), and provide thorough transcriptomic profiling and substrate

141 characterization data. We confirmed robust but much slower growth of the pyrite-supported cell
142 cultures ("py") compared to their positive controls (amended with sodium sulfide and containing
143 soluble $\sum H_2S$). Differential gene expression analyses (of cells harvested at their respective
144 exponential growth phases in "py" versus positive controls) revealed up to hundreds of fold
145 changes in the expression of genes encoding various types of cytochromes, LH complex
146 subunits, bacteriochlorophyll *a*, and enzymes involved in dissimilatory sulfur metabolism. We
147 have also proposed a model for pyrite oxidation by *A. vinosum* in the discussion.
148

149 ## Materials and Methods

150 *Strain, medium and culture conditions*

151 The strain of *A. vinosum* DSM 180 was obtained from DSMZ, Germany. Culture media
152 for *A. vinosum* was prepared following Pfenning's medium recipe with modifications that
153 removed compounds allowing for potential heterotrophic growth. Several types of media were
154 prepared for the experiments: one for the sulfur-free control, another for the positive controls,
155 and the last for the pyrite-amended cell cultures. Other than the sulfur source, these media are
156 identical in their compositions. Specifically, the positive control medium is amended with
157 $Na_2S{\cdot}9H_2O$, overall consisting of 1.7 mM of $CaCl_2{\cdot}2H_2O$, 250 mg/L of yeast extract, 6.5 mM of
158 NH_4Cl, 4.6 mM of KCl, 1 mM of $MgCl_2{\cdot}6H_2O$, 20 mM of HEPES, 35 mM of $NaHCO_3$, 5.1 mM
159 of KH_2PO_4 and 5 mM of $Na_2S{\cdot}9H_2O$. The "py" medium did not contain $Na_2S{\cdot}9H_2O$ but 750
160 mg/L of pyrite. The sulfur-free control contained neither $Na_2S{\cdot}9H_2O$ nor pyrite. In preparation of
161 the full media, we made two types of solutions (A and B) separately. Solution A was prepared
162 through boiling Milli-Q water (18.2 MΩ·cm), degassed with ultrapure N_2 gas during cooling
163 down. All salts except for the carbon and sulfur sources (i.e., $NaHCO_3$ and $Na_2S{\cdot}9H_2O$/pyrite)

164 and KH_2PO_4 were added to the degassed solution, which was further degassed using N_2 for ~45
165 min. A mineral mix (composition provided in Supplemental Information) was added to the
166 cooled solution A as a ratio of 10 μL/mL, following which trace amounts of concentrated 6N
167 HCl was added (at a ratio of 1 μL/mL before bottling in serum bottles sealed by rubber septa and
168 aluminum rings. The purpose of adding trace amounts of HCl is two-fold: facilitating the
169 dissolution of all the salts and resulting in a final medium (through mixing A and B) pH in the
170 range of 7.1-7.3. As a separate solution (B), boiled and N_2-degassed/cooled Milli-Q water was
171 sterilized using 0.2-μm syringe filters and stored in a sterile serum bottle, further bubbled using
172 ultrapure N_2 at room temperature for ~15 min. Immediately prior to sealing the bottles with
173 rubber septa, $NaHCO_3$ and $Na_2S{\cdot}9H_2O$ were added. The fast sealing can prevent loss of sulfide
174 and CO_2, keeping the medium composition close to the designated one. Full media was made by
175 mixing 90% of solution A into 10% of solution B by volume and adding 10 μL of ATCC
176 Vitamin mix per mL of full media through syringe filtering. Inoculations of the positive and
177 negative controls were carried by adding 1% (v/v) of the stock cell culture medium (a positive
178 control at mid-late exponential growth phase), and the initial total volume of cell cultures was
179 200 mL. Two types of negative controls were created: non-inoculated culture of pyrite-amended
180 medium, and inoculated culture of the sulfur-free medium (no sodium sulfide or metal sulfide
181 added). The pyrite tested in the experiments was obtained from Fisher Scientific (as high purity
182 naturally occurring pyrite FeS_2, further pulverized and washed/sterilized using ethanol). X-ray
183 diffraction and transmission electron microscopy coupled with energy dispersive spectroscopy
184 analyses confirmed the pure pyrite (FeS_2) phase. Inoculation of the pyrite-amended medium was
185 done using a former pyrite cell culture (1%, v/v) to minimize potential sulfur carryover. The
186 pyrite-to-pyrite inoculation was also observed leading to slightly faster growth cycles of the

187 pyrite cell cultures through multiple rounds of experiments. All "py" cell cultures and positive
188 and negative controls were kept in a shaker incubator maintained at 30 ˚C and 100 rpm, under an
189 incandescent lamp with tungsten filament (100W, hyperspectral analysis of the light illumination
190 is included in Supplemental Information). We note that the addition of a low amount of yeast
191 extract (250 mg/L) is necessary to kick off the cell growth in the "py" samples. Cell growth was
192 observed in the negative control but was significantly lower than that in "py". The growth of the
193 cell cultures was monitored using optical density at 600 nm and DNA yields (see the following
194 section for DNA extraction and quantification). Bacteriochlorophyll a level of the cell cultures at
195 various times was also evaluated using an acetone-methanol extraction method coupled with
196 spectrophotometric analysis, but only in a comparative manner. It is noted that all the glassware
197 used in the experiments are acid-washed and thoroughly rinsed with DI water and Type-1
198 ultrapure water in our laboratory.

199 *Nucleic acids extraction and analysis*

200 DNA and RNA samples were recovered from the cell cultures using the GenElute
201 Bacterial Genomic DNA kit (Sigma Aldrich) and the RNeasy Mini kit (Qiagen), respectively. In
202 sampling, 1 mL aliquots of the cell culture medium were removed using N_2-purged syringes. In
203 the case of sampling for RNA extraction, RNAProtect® was immediately added to the aliquots
204 and incubated for 5 min. The sampled aliquots (with/without RNAProtect®) were then
205 centrifuged at 5,000 g for 10 min, following which the supernatant was discarded. The cell
206 pellets were maintained at -80 ˚C until the DNA/RNA extraction was done. For the DNA
207 extraction, the cell pellets were extracted using the Gram-positive quick protocol (which was
208 found to be more efficient than the Gram-negative protocol for *A. vinosum*) from the GenElute
209 Bacteria Genomic DNA kit manual. For the RNA extraction, the cell pellets were first lysed

210 following a protocol recommended by the RNEasy kit. The lysis solution was prepared by
211 mixing 10 µL of proteinase K (20 mg/mL) and 100 µL of lysozyme (15 mg/mL) in the TE buffer
212 solution (10 mM of TrisHCl, 1 mM of EDTA, and pH 8). Enzymatic digestion was carried out at
213 room temperature for 10 min in a rotary shaker. The RNeasy extraction was subsequently done
214 using the lysate following the RNeasy Mini kit instructions. For the RNA extraction, DNA
215 removal steps are included in the kit instructions. (We have tested multiple RNA extraction
216 protocols, and the RNeasy was shown to be the most robust and consistent for *A. vinosum*.)
217 Quantification of DNA and RNA, respectively, was done using Nanodrop® One
218 spectrophotometer and Qubit fluorometer, while quality control was done through 260/280 and
219 260/230 ratios and through DIN and RIN analysis using Tapestation 2200.

220 *Transcriptomic sequencing and bioinformatics*

221 The Illumina platform technology was used to sequence both "py" samples and positive
222 controls cDNA libraries, which were derived from total RNA cultures in their respective mid-late
223 logarithmic phase (the time point for the samples used for transcriptomic sequencing are marked
224 in **Fig, 2**). We have included triplicate samples for each sample type and triplicate sequencings
225 for each sample. The sequencing was performed using a 400M read flow cell NextSeq 2000
226 cartridge with a 150 bp-end read length. To ensure the quality of the samples, FastQC was
227 utilized to confirm their integrity. Trimmomatic software[56] was employed to trim reads of
228 adapters, low-quality bases, and fragments smaller than 60 bp from raw data. The resulting high-
229 quality trimmed reads were then aligned to the reference genome of *A. vinosum* (Genbank:
230 CP001896.1) using Bowtie2 software[57], which can generate an indexed version of the reads. For
231 transcript quantification, the paired-end indexed data of both positive control and pyrite samples

232 were used with RSEM software. Furthermore, the DESeq2 package[58] of the R was used for data
233 normalization and differential analysis of the statistical processing of the data.

234 *Dissolved species characterization*

235 Growth of bacteria in the positive controls and "py" samples was tracked indirectly by
236 measuring the concentrations of dissolved iron, sulfide, and sulfate in the medium solution over
237 time. Collected samples for sulfide measurements were processed immediately to minimize
238 sulfide escape from solution over time. A 100 μL aliquot of each sample was reacted with 40 μL
239 of excess zinc chloride solution (~ 100-fold of the molar amount of sulfide) to form metastable
240 ZnS. Sulfide measurements were done using the methylene blue method which involves reagent
241 to react with any sulfide present including the precipitated ZnS to yield equimolar amount of
242 methylene blue. The concentrations of the generated methylene blue were then measured by
243 tracking the absorption at 665nm using a MultiSkan UV-Vis spectrophotometer. Specifically, the
244 zinc chloride-stabilized mixture was reacted with 250 μL of sulfide 1 reagent and 250 μL of
245 sulfide 2 reagent (obtained from Hach) and diluted with 400μl MQ water to generate a ~1:10
246 dilution. The mixture was placed in a rotary shaker for a period of 10 min before the UV-vis
247 measurement. In the case of sulfate measurement, a nitrogen purged syringe was used to
248 collected aliquots of samples that were diluted 1:10 with Milli-Q water and subsequently filtered.
249 Sulfate measurements were performed using a Dionex ICS-2100 ion chromatography system and
250 quality control (QC) was performed by jointly running a standard curve made with sodium
251 sulfate. Concentrations of major elements in the control and sample solutions were measured
252 using inductively coupled plasma (ICP)-optical emission spectroscopy (OES) or mass
253 spectrometry (MS) depending on the concentration levels. The aliquots of the medium solution
254 for the ICP runs were diluted 100-fold using 2% HNO_3 solution and filtered (0.2 μM cutoff) into

255 15ml conical centrifuge tubes. Samples were analyzed by ICP-OES (iCAP 6500, Thermo Fisher
256 Scientific, Waltham, MA) and ICP-MS (7700 Series, Agilent, Santa Clara, CA) to determine the
257 concentration levels for a group of elements (including Ca, K, Mg, Na, P, S, Zn, Fe, Ni, Mo, and
258 Cu). To validate measurements, a blank and standard reference materials (NIST-SRF 1570a and
259 1547, Metuchen, NJ) were prepared and analyzed. Spikes at different concentrations were used
260 to obtain the standard working curve. The recovery rate of all the tested elements was above
261 99%. Yttrium (Y) was used as an internal standard and a continuing calibration verification
262 (CCV) sample was analyzed every 15 samples.

263 *Solid-phase characterization*

264 Solid phases in the cell-free negative control and "py" samples were analyzed using X-
265 ray diffractometry (XRD), transmission electron microscopy (TEM), and X-ray photoelectron
266 spectroscopy (XPS). The solid pellets recovered through centrifugation and supernatant removal
267 were processed using 0.1% Triton X-100 solution containing 10 μg/mL of lysozyme and 10
268 μg/mL of proteinase K to remove the bacterial cells and biomolecular debris. The pellets were
269 sonicated in the processing solution for 45 min at room temperature. The solid particles were
270 then separated by centrifuging the digestion mixture at 10,000 × g for 5 min at room temperature
271 and removing the supernatant. The separate solid particles were washed twice with 0.1% Triton-
272 X. All operations were carried out in an anaerobic chamber in sealed containers prepared to
273 prevent sample oxidation. The biomass-digested solid particles were fractioned for XRD, XPS,
274 and TEM analyses. The sample preparation for the XPS specimen involved drying the separated
275 particles on top of a glass slide under anaerobic conditions. The XRD specimen were prepared
276 similarly but the final slides were finished by a layer of grease on top of the dried particle sample
277 to protect the samples from oxidation. In the case of TEM sample preparation, 5 μL of anoxic

278 water was added to the gold grid with ultrathin carbon film and then 10 μL of particle suspension
279 was added. The XPS spectra were collected using a PHI Quantera SXM (ULVAC-PHI, Japan)
280 with a hemispherical energy analyzer and a monoenergetic X-ray source (Al Kα: 1486.6 eV).
281 The survey spectra were collected at 25 W/15 kV with a spot size of 100 μm, 45° take-off angle,
282 and 280 eV pass energy. A 69-eV pass energy with 0.125 eV scan step was chosen for high
283 resolution spectrum acquisition. The high-resolution XPS spectra were fitted using Multipak
284 software, with the charge correction based on adventitious C 1s at 284.8 eV. The XRD samples
285 were analyzed using a Rigaku MiniFlex II Desktop X-ray Diffractometer which operates uses
286 Cu-tube Ka radiation at 30kV and 15mA at a scan rate of 1.5 degrees/minute. The TEM data
287 were gathered using a JEOL JEM 2100 S/TEM at the Nanoscale Characterization and
288 Fabrication Laboratory located in Virginia Polytechnic Institute and State University. The
289 instrument was operated at 200 kV, and TEM bright field images were taken using a Gatan
290 Ultrascan 1000XP CCD camera. The collection of selected area electron diffraction patterns was
291 performed utilizing a Gatan Orius 833 slow scan CCD camera. Furthermore, scanning TEM
292 (STEM) mode was used to obtain Energy dispersive X-ray spectroscopy (EDS) data using a
293 JEOL genuine 60 mm2 Silicon Drift Detector.
294

295 ## Results

296 *Growth profiles*

297 In positive controls, it takes ~120 h for the cell culture to reach the end of logarithmic
298 phase, yielding a cell density of ~ 9.4×10^6 cells/mL, and the stable phase spans from 140 h to
299 400 h with comparable optical density at 600 nm (OD_{600}) and pigmentation intensity throughout
300 the period (**Fig. 2**). The cell density was estimated through correlating the OD_{600} and cell

301 counting results. The "py" cell culture has a longer lag phase than the positive control and rose to
302 a cell density of ~2.5 × 10^6 cells/mL, about one quarter of that of positive controls, at ~240 h. We
303 have identified further (slower) growth for "py" cell cultures after the OD reached a local
304 maximum (at ~ 240 h), and such growth lasted till ~550 h. The cell growth in "py" was also
305 quantified using the samples' DNA yields, showing a maximum of ~ 4 ng/μL at ~ 550 h,
306 consistent with the OD data. Depletion of sulfide was recorded at ~120 h for positive controls
307 and the production of sulfate through sulfur oxidation reached a maximum of 0.7 mM (**Fig. 2**).
308 For "py", sulfide concentrations remained below the detection limit while sulfate reached up to
309 ~20 μM within the monitored period of up to 1000 h. The soluble iron concentrations in "py"
310 showed a spike at ~ 550h. The timing of the spike resonates strongly with that of maximum OD
311 and DNA yield. It is noted that the maximum level of iron concentrations in "py" is still rather
312 low, ~ 600 ppb, compared to that (~ 200-300 ppb) in the controls.

313 *Transcriptomic sequencing and differential gene expression analysis*

314 The genome for *A. vinosum* has been reported to be 3.8 Mb encoding ~3,300 proteins and
315 a similar number of genes (Weissgerber *et al.* 2011). The transcriptomic sequencing analysis of
316 the "py" and positive control samples identified a total of 3302 genes, in line with the previous
317 report. Through differential gene expression analysis of "py" vs. positive controls, and using
318 $\log_2FC > 2$ or $\log_2FC < -2$ as well as $P < 0.05$ as the cutoff, we have identified a total of 80
319 upregulated and ~100 downregulated genes (**Fig. 3** and **Table 1**). Among these top differentially
320 regulated genes, ~15% of the upregulated and 7% of the downregulated are associated with
321 redox-active proteins such as cytochromes, hydrogenases, reductases, and others with Fe-S
322 motifs. Sulfur metabolic genes accounted for 2% of the upregulated and 6% of the
323 downregulated (using $\log_2FC > 2$ or $\log_2FC < -2$ as the cutoff). Genes associated with signal

transduction and transcription regulation accounted for 8% of the upregulated and 3% of the downregulated. Photosynthetic RC-related genes were exclusively downregulated (except for those associated with carotenoid biosynthesis), accounting for 9% of the downregulated sequences. Interestingly, 3% of the upregulated genes are associated with metal efflux controls, and 4% (also of the upregulated) are concerned with cellular appendages sequences, including flagella, fimbriae and pilin genes.

Among the most differentially regulated genes, we identified a collection of cytochrome-related genes, whose fold change for the upregulated ones are up to ~ 200. For example, Alvin_1092 and Alvin_1093, which encode flavocytochrome *a* and *b*, involved in hydrogen sulfide-dependent cytochrome *c* reduction, are upregulated by up to 175-fold; and Alvin_0020 and Alvin_0023, which encode a diheme cytochrome *c*, are upregulated by ~ 47-fold. Others in the upregulated list include Alvin_0021, encoding a cytochrome *b*561 (which is in the region dominantly encoding *c*-type cytochromes), Alvin_2307, encoding a Ni/Fe hydrogenase *b*-type cytochrome subunit, Alvin_2452-2454, encoding three formate dehydrogenase subunits, and Alvin_2989, encoding NAD(P)H dehydrogenase. The downregulated genes, excluding those tabulated in Tables 1-3 (which will be discussed in the following paragraphs), include several genes related to dehydrogenases found in carbon metabolism cycles, such as Alvin_0315, Alvin_0804-805, and Alvin_2427-2428. The former three encode glyceraldehyde-3-phosphate dehydrogenase, pyruvate dehydrogenase complex dihydrolipoamide, and 2-oxoacid dehydrogenase E1 subunit, respectively, whereas the latter two encode NADH dehydrogenase subunits.

The genes encoding metal ion transporters, Na^+/H^+ antiporter, and flagella, fimbriae, and pili components, are also in the most differentially regulated list. For metal ion transporters,

347 Alvin_0013-0015 likely represent components of efflux transporters of the RND and CzcA
348 families, and Alvin_0019 and Alvin_1521 are respectively associated with FieF Iron efflux
349 pump and a periplasmic efflux protein. The upregulated flagella-associated genes include
350 Alvin_1952-1954, encoding FlaG, a flagellar hook-associated protein, and FliS, respectively.
351 Alvin_3016 is associated with fimbriae biogenesis (i.e., FimT) and Alvin_1186 with a pilin
352 protein PilT.

353 The expression of genes associated with light harvesting and dissimilatory sulfur
354 metabolism pathways showed consistently distinct patterns for "py" versus positive controls
355 (**Tables 2-3** and Supplemental **Figs. S1-S2**). In the case of light harvesting complexes, genes
356 relevant to biosynthesis of LH1, LH2 and reaction center components were exclusively
357 downregulated. Specifically, the gene clusters, *pufC*, *pufM*, and *pufL*, which are co-transcribed
358 with three sets of *pufA* and *pufB* genes, encoding LH1 apoproteins, were suppressed by various
359 levels, up to 10-fold (Alvin_2547-2555). The upstream *pufH* along with adjacent genes,
360 encoding photosynthetic complex assembly proteins and a hypothetical protein, was also slightly
361 suppressed (Alvin_2634-2637). The genes associated with LH2 apoproteins were suppressed the
362 most, by up to 115-fold (Alvin_0703-0706, and 0708-0709). By comparison, genes related to
363 biosynthesis of Bchl*a* and carotenoids were either moderately suppressed or enhanced in
364 expression (Alvin_1182-1183, 2556, 2561-2563, 2638-2643, and 2564-2570). In the case of
365 dissimilatory sulfur metabolism, we evaluated the expression of three genes related to Sgp
366 proteins and found upregulation of Alvin-1095 (representing SgpA) by ~ 42-fold in the
367 differential analysis of "py" vs. positive controls. The other two genes, Alvin_0358 and
368 Alvin_1325, were either slightly downregulated or unchanged. By comparison, *dsr* genes are
369 exclusively downregulated except for *dsrC.* Specifically, *dsr*A/Alvin_1251 and

370 *dsr*B/Alvin_1252, which form a *dsrAB* complex, show a ~22-fold expression suppression. The
371 other complex within the *dsr* loci is *dsrEFH*, from which *dsrE*/Alvin_1253 decreases by 11-fold
372 and *dsrF*/Alvin_1254 by 7-fold. The genes coding membrane-bound Dsr proteins were also
373 downregulated, by ~ 4-fold for *dsrJ/*Alvin_1260, 4-fold for *dsrO*/Alvin_1261, and 3-fold for
374 *dsrP/*Alvin_1262. The only gene that remained relatively unchanged in its expression level is
375 *dsrC*/Alvin_1256. Besides *dsrC*, there are four more genes annotated as TusE/DsrC/DsvC family
376 sulfur relay proteins, namely Alvin_0028, Alvin_0345, Alvin_0732 and Alvin_1508[18], which are
377 respectively upregulated by ~ 2-, ~ 2-, and ~ 4-fold, and downregulated by ~ 7-fold. In the *sox*
378 loci, genes encoding SoxYZ complex were upregulated by 5-fold, while the rest of the *sox* genes
379 seemed unaffected in terms of expression levels.

380 It is important to highlight that a considerable portion of the highly
381 upregulated/downregulated genes, ~30% of the upregulated and ~23% of the downregulated
382 genes, were considered hypothetical proteins or domains of unknown function (DUF)
383 (Supplemental **Table S1**). A taxonomy analysis was carried out to infer how prevalent and
384 conserved the sequences of these genes might be within γ-Proteobacteria. In the taxonomy
385 analysis, the percentage of hits from reported γ-Proteobacteria sequences among the total hits
386 was presented, indicative of the potential relationship of the unknown protein to γ-
387 Proteobacteria. The analysis shows that 14 out of 18 upregulated genes and 16 out of 25
388 downregulated hypothetical sequences show ~ 90% or higher blast results. We have also
389 identified certain motifs (e.g., signal peptide) and transmembrane domains in some of these
390 unknown protein sequences.

391 *Pyrite substrate analysis*

The pyrite recovered from the cell culture medium showed irregularly shaped particles with wide-ranging dimensions of ~100 nm to several microns (μm) (**Fig. 4**). In these biological pyrite samples, we observed apparent amorphous domains, with no electron diffraction patterns and richer in sulfur compared to the highly crystalline domains. Based on the d-spacings obtained using the electron diffraction micrographs, the solids in the *A. vinosum* culture consist of pyrite, and likely pyrrhotite and elemental sulfur. Although different interpretations may be made based on the electron diffraction patterns alone, the corresponding XPS analyses provide extra constraints on the Fe and sulfur valence states and bonding as well as sulfur-to-iron composition ratios (**Fig. 5**). The results showed that only Fe(II) was present in both abiotic and biotic pyrite samples. An asymmetric fit was performed on the iron region of the spectra to calculate the relative abundance of the species identified. The abiotic control (pyrite) showed a main 2p3/2 peak at 706.72 eV, matching the binding energy for Fe(II) valence electrons in pyrite, along with a satellite peak at 707.95 eV, likely resulting from surface defects. The "py" sample (biotic sample) had a peak at 706.37 eV in the iron region, with a satellite peak at 707.58 eV, which may indicate the presence of Fe(II)-O speciation (i.e., adsorption of soluble Fe(II) on solid surfaces). Both samples displayed the same oxidation state of Fe(II), with no evidence of Fe(III) and its satellite peak. The surface composition of both materials was extremely similar, with a small increase in the dominance of the Fe(II) 2p3/2 peak, from 65% in the control to 67% in the biotic sample. The fit of the sulfur region spectra required doublet peaks, with the area of the 2p3/2 peak set to be twice that of the p1/2 and the distance between them set at 1.18 eV. The abiotic control showed four different sulfur species, including S^{2-} at 161.14 eV for p3/2, with an orbital split p1/2 peak at 162.32 eV, polysulfide at 164.1 eV for p3/2, with a p1/2 peak at 165.28 eV, disulfide at 162.1 eV for p3/2, with a p1/2 peak at 163.28 eV, and a fourth unidentified peak

415 at 162.34 eV and matching orbital split at 163.52 eV. The fourth peak fell 0.14 eV away from the
416 main disulfide peak, but its corresponding species is unknown. The biotic sample showed three
417 sulfur species, including S^{2-} at 161.3 eV and 162.48 eV, disulfide at 161.82 eV and 163 eV, and
418 polysulfide at 163.7 eV and 164.88 eV. Both the control and biotic pyrite samples showed the
419 presence of monosulfide, disulfide, and polysulfide. However, the unidentified peak close to the
420 main disulfide peak in the control disappeared in the biotic sample. Upon closer comparison, the
421 biotic sample showed increases in the abundance of polysulfides from 9% in the control to 15%
422 in "py", of monosulfide from 5% to 15%, and of disulfide from 47% to 70%. Nevertheless,
423 considering that apical, bridging, and terminal ligands cause a significant peak position shift, and
424 including the unknown 0.14 eV peak as a variation of disulfide, the biotic sample disulfide
425 decreased from 85% in the control to 70% overall. The relative abundances of each iron/sulfur
426 species were estimated based on the XPS analysis, and interestingly, the overall sulfur-to-iron
427 ratio increased greatly for the "py" samples, reaching ~12.6, compared with that for the negative
428 control samples, ~ 3.9.
429

430 ## Discussion

431 The cell growth profiles and transcriptomic analysis results revealed significant changes
432 in the cells' major metabolic pathways, including electron transport, RC and LH complex
433 biosynthesis, and sulfur oxidation. We have specifically discussed these changes in the following
434 section. Combining these molecular biological analyses with the pyrite substrate analyses, we
435 have also proposed mechanisms of interaction between *A. vinosum* and pyrite that enabled the
436 bacterial cells' autotrophic growth.

437 *Key roles of cytochromes in A. vinosum-pyrite electron transfer*

438 The genome of *A. vinosum* encodes a wide range of cytochromes that are known to play
439 key roles as diffusible electron carriers, dissimilatory sulfur metabolism enzymes, and
440 hydrogenases, etc. In the current study, up to ~ 200-fold upregulation was identified for a
441 number of genes related to *c*-type and, to a lesser extent, *b*-type cytochromes in the "py" cell
442 cultures. Further analyses revealed that some of the upregulated genes are associated with
443 soluble or membrane-bound *c*-type cytochromes or flavocytochromes (Alvin_1093, 0020, and
444 0023), previously classified as diffusible electron carriers. It is noted that Alvin_1093 is one of
445 the top upregulated genes (expression increased by ~ 175-fold) in the "py" cells. Alvin_1093 and
446 Alvin_1092 (upregulated by ~ 75-fold) encode a heterodimer consisting of a 21 kDa diheme
447 cytochrome *c* subunit (FccA) and a 46 kDa flavin-binding subunit (FccB) in *A. vinosum* (Brune
448 1995). Although soluble *c*-type cytochromes were shown to catalyze the oxidation of sulfide to
449 sulfur or polysulfides *in vitro*[22], the roles of FccA and FccB in *A. vinosum* remain unresolved. As
450 pointed out in Weissgerber *et al.*[18], mutants in which the genes *fccAB* are inactivated by a
451 kanamycin cassette still oxidize sulfide with rates similar to the wild type[22]. Some sulfide-
452 utilizing green sulfur bacteria, e.g. *Chlorobium luteolum*, and purple sulfur bacteria, e.g.
453 *Thiocapsa roseopersicina*, *Thiococcus pfennigii*, and *Allochromatium warmingii*, do not produce
454 flavocytochrome *c*, which is an additional hint that flavocytochrome *c* is not essential for sulfide
455 oxidation[4]. Interestingly, Alvin_1093 along with Alvin_1092, 0020, and 0022-0023 showed
456 distinctive regulation patterns for the pyrite-supported cells in this study than the elemental
457 sulfur (S^0)-supported cells (also of *A.vinosum* DSM180) in a previous study[59] (Supplemental
458 **Table S2** and datasets). Specifically, Alvin_0020, 0022, and 0023 were significantly suppressed
459 in the S^0-supported, photoautotrophically grown cells versus their positive controls using soluble
460 sulfide, whereas Alvin_1093 was slightly enhanced[59]. Such evident variations strongly indicate

461 that Alvin_0020, 0022-0023, and 1092-1093 have played particularly important roles in the *A.*
462 *vinosum*-pyrite interactions in the current study (further discussion of Fcc is provided in the
463 "dissimilatory sulfur metabolism" section). Up to 41-fold upregulation of Alvin_1095, associated
464 with a 4-heme *c*-type cytochrome, was also observed although the component's function and
465 pathway have not been resolved.

466 We further evaluated whether cytochromes, especially those with multihemes may play a
467 role in the *A. vinosum* cell-pyrite electron transfer, linking intracellular energy reactions to the
468 oxidation of solid pyrite external to the cells. The phenomenon of extracellular electron transfer
469 (EET) has been demonstrated in over ~ 100 microbes to date, perhaps most notably in *Geobacter*
470 *sulfurreducens* and *Shewanella oneidensis*, where a network of multiheme *c*-type cytochromes
471 on the inner membrane, periplasm, and outer membrane couple intracellular energy reactions
472 with the use of external solid electron donors or acceptors[60-63]. Multiheme cytochromes (MHCs)
473 in particular are key players in extracellular electron transfer[62], as the proximity and arrangement
474 of hemes can allow efficient intraprotein electron transfer[64]. We identified 43 putative *c*-type
475 cytochromes in *A. vinosum* based on the presence of CXXCH heme *c* binding motifs, and of
476 these 18 were putative MHCs (containing multiple CXXCH motifs): specifically, 11 × diheme, 1
477 × 3-heme, 3 × 4-heme, 1 × 7-heme, and 2 × 8-heme cytochromes (Supplementary **Table S3**).
478 Some of the larger ones (e.g. 7 or 8-heme) in particular, and various others, have no annotated
479 functions; the expression of these larger MHCs was exclusively enhanced in the "py" cells. The
480 remaining 25 are putative monoheme *c*-type cytochromes. We also probed these genes for the
481 presence of LXXC lipid binding motifs and/or signal peptide, as both periplasmic and
482 membrane-associated cytochromes are required for extracellular electron transfer. LXXC is a
483 lipoprotein consensus sequence for signal peptidase II found in key outer membrane

484 cytochromes in *S. oneidensis*[65]. SignalP[66] can detect 5 types of signal peptides, i.e., a protein can
485 enter the cell's secretory pathway, where it may be localized to the inner membrane, exported to
486 periplasm, or localized to the outer membrane. In total, 19 out of 43 putative cytochromes
487 contained LXXC lipid motif, and 21 were detected by SignalP; and 8 were detected for both. The
488 fact that multiple cytochromes are potentially associated with the inner or outer membrane (with
489 others not identified here possibly being soluble electron carriers) is promising towards
490 identifying a potential cytochrome network for extracellular electron transfer in *A. vinosum*.
491 Experimental evidence will be required to confirm the cellular localization of cytochromes in *A.*
492 *vinosum*, and whether they contribute to extracellular electron transfer. As a disclaimer, other
493 cytochromes of interest may exist, e.g. those without heme *c* motif (CXXCH), or those not
494 detected by the LXXC lipid motif or by SignalP. In total, 10 putative *c*-type cytochromes
495 (including an 8-heme, 2 diheme and 7 monoheme) were upregulated in the "py" cells and may be
496 of particular interest towards investigating the coupling of carbon fixation at the inner membrane
497 to the oxidation of pyrite outside the cell.

498 *Less important Roles of LH and RC complex components?*

499 Another major change identified in the "py" cells is the downregulation of photosynthetic
500 genes related to the biosynthesis and assembly of LH and RC components (**Table 2** and
501 Supplemental **Fig. S1**). As a recap, the expression of *puc* clusters encoding LH2 apoproteins
502 were significantly suppressed, by up to ~70 fold; the *puf* clusters and genes related to
503 biosynthesis of Bchl *a* were also downregulated, by ~ 8-10-fold for the former and by ~ 2-fold

Soluble source: Na_2S with an initial concentration of 5 mM

Solid-phase source: Fe_2S with a loading of ~ 4 g L^{-1}

Assuming the ave particle size is 100 μm (radius) and the surface 10 nm layer is accessible for direct interactions with bacterial

Then the accessible concentration of pyrite is:

$$\frac{4\ \mathrm{g{\cdot}L^{-1}}}{120\ \mathrm{g{\cdot}mole^{-1}}} \times \frac{4\pi r^2 \cdot d}{4/3\pi r^3} = \frac{d}{r} \times 0.1\ mole{\cdot}L^{-1} = 0.01\ mM$$

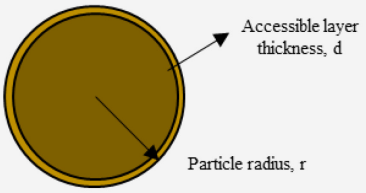

22

504 for the latter. The only genes not affected or enhanced in expression within the photosynthetic
505 category are those representing carotenoids biosynthesis (Alvin_2564-2570). It is still premature
506 to conclude what has caused the extensive downregulation of the photosynthetic LH- and RC-
507 related genes in the "py" cells. A most likely reason might be that the growth rate of the "py"
508 cells was limited by the electron supply and its connection to the carbon fixation pathway, and
509 thus, the demand for higher-density LH and RC complexes was no longer existent. We have
510 compared the availability of solid-phase pyrite versus soluble Na_2S as an electron donor (shown
511 below) assuming that the electron scavenge was restricted in surface layer of pyrite and found ~
512 2-3 order of magnitude difference in their effective concentrations.

513 It is noted that the relationships among the RC complex, sulfur-oxidation pathway, and
514 carbon fixation pathway remain are not fully understood. In other words, it is unknown whether
515 the reactivity of RC complex is specifically affected by the electron donor source. If so, the
516 possibility of bypassing the LH-RC complex by the bacterial cells when using an alternative
517 electron source cannot be ruled out. We further evaluated the expression of genes related to
518 ribulose 1,5-biphosphate carboxylase/oxygenase (RuBisCO) in the "py" and positive control
519 cells as both types grew autotrophically with bicarbonate as the sole carbon source. *A. vinosum*
520 possesses two complete sets of genes encoding for RuBisCO subunits: the large subunit
521 RbcA/RbcB represented by Alvin_1365-1366 and the small one RbcS/RbcL represented by
522 Alvin_2749-2750[67]. Opposite trends have been observed for the two sets of RuBisCO genes in
523 the "py" cells, with Alvin_1365-1366 downregulated by at least 10-fold and Alvin_2749-2750
524 moderately upregulated by ~ 2-fold. According to the gene arrangement, the *rbcAB* gene belong
525 to IAq-form RuBisCO genes, typically associated with *cbbQ* encoding proteins affecting
526 RuBisCO activity[68], whereas the *rbcSL* genes are IAc-form RuBisCO genes[69]. Besides the

527 RuBisCO genes, *A. vinosum* harbors a gene encoding an IV-type RuBisCO-like protein (RLP)
528 (Alvin_2545), the expression of which decreased just slightly in the "py" cells. It remains
529 unclear what roles such RLPs play in *A. vinosum* metabolism, but likely not involved in RuBis-
530 dependent CO_2 fixation[70,71].

531 An alternative explanation for the probable "shutdown" of LH and RC, other than the
532 electron donor restriction, might be that the cells have established a less "expensive" pathway for
533 obtaining energy to drive their carbon fixation and growth. Regarding what other pathways may
534 be possible for *A. vinosum* cells to capture light energy, here we present a new hypothesis that
535 requires further experimental evidence. In this hypothesis, we assume that the electron transfer
536 from the extracellular pyrite substrate can be driven by both photochemical and non-
537 photochemical reactions to support CO_2 fixation and these mechanisms do not involve RC
538 complexes in *A. vinosum* (**Fig. 6**). There are obvious energy and nutrient appeals for *A.vinosum*
539 to enable such cell-pyrite interactions, which are further discussed in the "hypothetical model"
540 for pyrite oxidation by *A. vinosum*.

541 *Dissimilatory sulfur-oxidation metabolism*

542 For genes encoding major enzymes (likely) involved in dissimilatory sulfur metabolism,
543 we have observed opposite trends in their differential expressions (in "py" vs. positive control),
544 primarily divided by associated pathways of the relevant enzymes (**Table 3** and **Fig. S2**). We
545 will first discuss the genes representing Fcc and Sqr, respectively, although their roles in
546 dissimilatory sulfur-oxidation have not been fully resolved. It has been pointed out in our former
547 discussion on cytochromes that, FccA and FccB, the two subunits constituting an enzyme
548 catalyzing sulfide oxidation and a cytochrome reduction in the periplasm, are likely key in
549 enabling the *A. vinosum*-pyrite electron transfer. Chen *et al.*[72] provided a detailed illustration of

550 Fcc structures, which consist of a glutathione reductase-like flavin-binding subunit and a diheme
551 cytochrome subunit. Specifically, the diheme cytochrome folds as two domains with an unusual
552 interpropionic acid linkage joining the two heme groups in the interior of the subunit; and a
553 tryptophan, threonine, or tyrosine side chain may provide a partial conduit for electron transfer to
554 one of the heme groups located ~10 angstroms from the flavin. This structural configuration of
555 FccA or B cannot rule out the possibility of it bridging membrane-bound pyrite oxidation to
556 periplasmic metabolisms other than oxidizing pyrite within the periplasmic space. Meanwhile, *A.*
557 *vinosum* contains two membrane-bound Sqr enzymes belonging to types IV (Alvin_2145) and VI
558 (Alvin_1195)[59]. Sqr belongs to a family of FAD-dependent oxidoreductases utilizing a motif of
559 Cys-S-S-Cys as the key redox site[73]. Sqr has been previously identified to reduce the quinone
560 pool present in the photosynthetic or plasma membranes of purple bacterial cells and was
561 proposed as candidate proteins for oxidizing sulfide[22,74]. In the case of *Rhodobacter capsulatus*,
562 polysulfides were identified as main reaction products *in vitro*. In our current study, opposite
563 trends were observed in the differential gene expressions ("py" versus positive control) for
564 Alvin_2145, encoding type IV SqrD (upregulated by ~ 4.5-fold) and for Alvin_1195, encoding
565 type IV SqrF (downregulated slightly). A correlation between the occurrence of SqrD and the
566 production of intracellular sulfur globules has been suggested previously[23] mainly through
567 observations that *sqrD* genes are present in members of Chromatiaceae but absent in species of
568 Ectothiorhodospiraceae that exclusively produce extracellular sulfur globules. Relevant to this
569 discussion, we identified sulfur-rich amorphous phase in the biologically reacted pyrite in the
570 TEM analysis. However, we have not confirmed the source of this possibly polymeric sulfur
571 phase, i.e., whether it was intracellular or pyrite oxidation product. The downregulation of
572 Alvin_1195 is consistent with previous understanding that SqrF is involved in optimizing cell

573 growth at high sulfide concentrations[23], which was not the case for the "py" cell cultures in this
574 study. It is still unknown if the cells grown on pyrite in this study can form sulfur globules in the
575 periplasm. The genes representing the envelope proteins of such sulfur globules (i.e., SgpA,
576 SgpB and SgpC) showed interesting patterns in differential gene expression analysis, however.
577 Specifically, SgpA, SgpB and SgpC are encoded by Alvin_1905, Alvin_0358 and Alvin_1325,
578 respectively. SgpC plays an important role in globule expansion, whereas SgpA and SgpB can be
579 replaced by each other to some extent[75,76]. In our study, Alvin_1905 and Alvin_0358 were
580 slightly downregulated, and Alvin_1325 remained unchanged. We note here that the expression
581 of genes representing Sgp were not apparently suppressed in the "py" cell cultures compared to
582 positive controls, which creates a sharp contrast with the trends previously reported for "S^0-
583 supported" cell[59].

584 The general trend for the three clusters of *sox* genes is moderate upregulated or relatively
585 unaffected in the "py" cells (compared to positive controls). It is noted that the Sox protein
586 complex is localized in the periplasm, which differs from the location of Dsr proteins. Although
587 Dsr proteins were implicated as key participants in oxidation of sulfur globules, genes related to
588 Dsr are downregulated in the current study [except that *dsrC* (Alvin_1256) remained relatively
589 unchanged in its expression level]. In fact, a review chapter on dissimilatory sulfur metabolism
590 in purple sulfur bacteria pointed out that purple non-sulfur bacteria, including those able to
591 oxidize elemental sulfur lack *dsr* genes[28] and the *A. vinosum* cells grown upon external sulfur,
592 showed significant downregulation in their *dsr* genes[59]. Combined with the latest results in this
593 study, it is strongly suggested that Dsr are not highly involved in metabolism of external solid
594 substrate of sulfur. Dsr proteins are largely localized in the cytoplasm, with a transmembrane
595 complex (DsrMKJOP). It is likely that the specific locality and connection to photosynthetic

596 electron transport chains[77] of Dsr proteins make it difficult for most of them to participate in
597 pyrite utilization if pyrite oxidation occurred largely outside the cells and the produced
598 intermediate sulfur species differed from those produced through soluble sulfide oxidation. It is
599 noted that while the *dsr* genes are transcribed as one single element, *dsrC* has an additional
600 independent promoter site[78], pointing at a special function of DsrC. Further, besides *dsrC*, there
601 are four more genes annotated as TusE/DsrC/DsvC family sulfur relay proteins, namely
602 Alvin_0028, Alvin_0345, Alvin_0732 and Alvin_1508. We observed upregulation by ~ 2-4-fold
603 for Alvin_0028, 0345, and 0732, and downregulation by ~ 8-fold for Alvin_1508.

604 The *dsr* gene expression data are consistent with the lack of sulfate in the "py" cell
605 culture medium (i.e., IC data), both of which suggest that *A. vinosum* cells might be capable of
606 oxidizing pyrite (or specifically pyrite surface-bound sulfur) to polysulfide or elemental sulfur,
607 but not able to further oxidize these sulfur species to sulfate. However, we also note that pyrite is
608 the sole sulfur source for the "py" cells, which may assimilate any sulfate produced from the
609 bacterial oxidation of pyrite. Further comparative kinetic studies are necessary to verify if *A.*
610 *vinosum* can oxidize pyrite to sulfate.

611 *Information from flagellum, fimbriae, and pilin genes*

612 We have singled out the genes associated with the biosynthesis of flagella, fimbria, and
613 pili because the expression of these genes was exclusively enhanced in "py". Many species of
614 purple bacteria swim with the assistance of flagella towards carbon/other nutrient sources and
615 light, using a complex set of chemosensory pathways[79]. The flagellum in bacterial cells is an
616 extremely complex structure, requiring the expression of genes encoding flagellar proteins to be
617 tightly regulated and ordered. The upregulation of Alvin_0408, 1188, 1569, and 3021 opens a
618 discussion on whether flagella, fimbria, and pili are involved in establishing physical contact

619 between *A. vinosum* cells and pyrite. Further, while a possible connection of flagellation and
620 substrate exploration and utilization has not been shown in bacterial cells, flagellar proteins were
621 recently speculated to be involved in direct physical contact with insoluble elemental sulfur for
622 oxidation in *Aquifex aeolicus*[80]. Overall, the extensive upregulation of flagellum-, fimbriae-, and
623 pilin-related genes manifests two key messages. First, mobility may be critical factor for *A.*
624 *vinosum* cells grown upon pyrite. High mobility may help the cells to move around easily to
625 either find the most "bioavailable" spots on pyrite or avoid the potential cytotoxic effects of
626 substrate surface radical species (which are common in photochemical reactions) and oxidation
627 products. Secondly, the enhanced expression of appendage genes also indicates that physical
628 contact is likely important in cell-pyrite interactions.

629 *Hypothetical model for pyrite oxidation by A. vinosum*

630 Based on the obtained solution, substrate, and gene expression analyses, we have
631 proposed a hypothetical model for pyrite oxidation by *A. vinosum* (**Fig. 6**). In this model,
632 physical contact of bacterial cells and pyrite particle surfaces is necessary for the pyrite-
633 supported cell growth. The utilization of pyrite is proposed to be driven by both photochemical
634 and non-photochemical processes. As pyrite has a band gap of 0.9 eV[81], the illumination setup
635 for the experiments is capable of exciting the charge separation in pyrite. Certain monoheme *c*-
636 type cytochromes may play a role as diffusible electron carriers, leading to oxidation of surface-
637 bound sulfur. Meanwhile, the periplasmic protein SoxY and SoxZ may bind to the sulfur on
638 pyrite surfaces and catalyze their oxidation. Both SoxYZ and diffusible electron carriers will
639 pass the electrons to a membrane-bound *c*-type cytochromes, which relays the electrons through
640 a quinone pool to cytochrome *b* to subsequently generate ATP. The various cytochromes
641 involved in the proposed pathways are yet to be identified, but from the upregulated list (based

642 on the gene expression analyses), several candidates with compatible reduction potentials may fit
643 into these roles. It is noted that there is no evidence that *A. vinosum* is capable of oxidizing
644 ferrous iron (separately tested in the current study). This hypothetical model well explains the
645 cryptic behavior of dissolved iron in the solution as the initial charge separation in pyrite is more
646 likely to oxidize structural Fe(II) to Fe(III), subsequently oxidizing the sulfur while being
647 reduced back to Fe(II); these cyclic reactions may lead to iron mobilization and/or monosulfide
648 reprecipitation depending on the locality of the sulfur involved in the process. Further
649 experimental evidence is required to validate this hypothetical model.

650 ## Conclusion

651 In this study, we showed that *A. vinosum* cells are capable of autotrophic growth using
652 pyrite as the source of sulfur and electron donors. The differential gene expression analysis along
653 with growth profile and substrate characterization data provided valuable insight into the
654 molecular mechanisms underlying the bacterial autotrophic growth. Up to ~ 200-fold
655 upregulation of genes encoding for a range of c-type and b-type cytochromes (including
656 multiheme ones) points to the high relevance of these proteins in scavenging and relaying
657 electrons from pyrite to key metabolic pathways. Conversely, the exclusive downregulation of
658 LH and RC complex components may suggest that the available electron donor source likely has
659 a dominant control over the bacterial cells' photosynthetic activity. The possibility that *A.*
660 *vinosum* may bypass some or all of the photosynthetic pathway and couple the electron
661 scavenging from pyrite directly to carbon fixation is not ruled out. The results of this study have,
662 for the first time, put the interplay of purple sulfur bacteria and transition metal sulfide chemistry
663 under the spotlight, with the potential to advance multiple fields, including metal and sulfur
664 biogeochemistry, bacterial extracellular electron transfer, and artificial photosynthesis.

665

666 ## Acknowledgements

667 This material is based upon work supported by the U.S. Department of Energy, Office of
668 Science, Basic Energy Sciences program under Award Number DE-SC0023251. This work used
669 shared facilities at the University of Texas at El Paso's Border Biomedical Research Center,
670 supported by the NIH-NIMHD (5U54MD007592) and at the Virginia Tech National Center for
671 Earth and Environmental Nanotechnology Infrastructure (NanoEarth), a member of the National

Nanotechnology Coordinated Infrastructure (NNCI), supported by NSF (ECCS 1542100 and ECCS 2025151). We are indebted to Dr. Lixin Jin, who has helped with the IC data requisition.

675 ## Figure Captions

676 **Figure 1.** Microbial sulfur oxidation-reduction patterns complicated by the presence of transition
677 metal species (TMs). In the absence of TMs, sulfate reducers reduce sulfate to sulfide/elemental
678 sulfur in couple with heterotrophy or mixotrophy, while sulfur-oxidizers oxidize
679 sulfide/elemental sulfur back to sulfate in couple with autotrophy. In the presence of TMs, TM
680 sulfide nanoparticles or thiometallate clusters may form within the cycle. It is unknown how the
681 formed TM-sulfur nanoparticles or complexes may affect the metabolic activity of associated
682 sulfur-oxidizers that depend on "free" sulfide to support CO_2 fixation.

683 **Figure 2.** *A. vinosum* growth profiles. Time profiles of (A) optical density (600 nm)
684 measurements of 10-fold diluted samples, (B) sulfate concentrations, (C) sulfide concentrations
685 (2-fold dilution), and (D) iron concentrations. The red dashed lines in (A) mark the
686 corresponding time points for the obtained transcriptomic sequencing data for "py" and positive
687 controls.

688 **Figure 3.** The volcano plot showing differential genes expressions in *A. vinosum* grown on pyrite
689 versus dissolved sulfide. We used the $\log_2FC < -2$ or $\log_2FC > 2$ as the cutoff; the upregulated
690 genes are displayed as green dots and downregulated genes as red dots.

691 **Figure 4.** HR-TEM displaying plate-like fragments of the solid substrate recovered from A.
692 vinosum-pyrite culture medium at the end of the experiments t > 1000 h. The solid materials
693 from the cell culture consist of a significant fraction of amorphous phases (B1), distinctive from
694 the abiotic controls. The biological samples may contain pyrrhotite (FeS), elemental sulfur (S),
695 and an unknown amorphous phase beside pyrite based on d-spacing estimation using the
696 obtained electron diffraction micrographs.

697 **Figure 5.** X-ray photoelectron spectroscopy (XPS) analysis of iron and sulfur speciation for
698 samples and controls (recovered at the end of the experiments t > 1000h). (A) Iron spectra for
699 biological pyrite-A. vinosum samples; (B) sulfur spectra for biological pyrite-A. vinosum
700 samples. (C) iron spectra for abiotic pyrite controls; and (D) sulfur spectra for abiotic pyrite
701 controls.

702 **Figure 6.** Proposed oxidation of pyrite driven by both photochemistry and diffusible and
703 membrane-bound cytochromes in A. vinosum. (A) Illustration of major proteins and other
704 components in PSB's RC complex. (B) proposed mechanisms for pyrite oxidation by A.
705 vinosum. (C) comparison of energy levels for PSB photosynthetic electron carriers vs. pyrite
706 conduction/valence bands (potential values obtained from reference 82 and 83).

707

References

1. Madigan, M.T., and Jung, D.O. 2009. "An Overview of Purple Bacteria: Systematics, Physiology, and Habitats." In The Purple Phototrophic Bacteria, 1–15. Springer, Dordrecht. https://doi.org/10.1007/978-1-4020-8815-5_1.

2. Cohen-Bazire, G., Sistrom, W.R., and Stanier, R.Y. 1957. "Kinetic Studies of Pigment Synthesis by Non-Sulfur Purple Bacteria." Journal of Cellular and Comparative Physiology 49 (1): 25–68. https://doi.org/10.1002/jcp.1030490104.

3. Imhoff J.F., Kyndt J.A., Meyer T.E. 2022. "Genomic Comparison, Phylogeny and Taxonomic Reevaluation of the *Ectothiorhodospiraceae* and Description of *Halorhodospiraceae* fam. nov. and *Halochlorospira* gen. nov." Microorganisms 10:295.

4. Brune, D. 1995. "Sulfur Compounds as Photosynthetic Electron Donors." In: Blankenship, R.E., Madigan, M.T., Bauer, C.E. (eds) Anoxygenic Photosynthetic Bacteria. Advances in Photosynthesis and Respiration, vol 2. Springer, Dordrecht. https://doi.org/10.1007/0-306-47954-0_39.

5. Hacking, K.A. 2015 "Characterisation of the LH2 Complexes of Allochromatium Vinosum." Doctoral dissertation.

6. Takahashi, M., and Ichimura, S. 1968. "Vertical Distribution and Organic Matter Production of Photosynthetic Sulfur Bacteria in Japanese Lakes." Limnology and Oceanography 13 (4): 644–55. https://doi.org/10.4319/lo.1968.13.4.0644.

7. Overmann, J.J., Beatty, T., and Hall, K.J. 1994. "Photosynthetic Activity and Population Dynamics of Amoebobacter Purpureus in a Meromictic Saline Lake." FEMS Microbiology Ecology 15 (3–4): 309–19. https://doi.org/10.1111/j.1574-6941.1994.tb00254.x.

8. Overmann, J., Beatty, J.T., and Hall, K.J. 1996. "Purple Sulfur Bacteria Control the Growth of Aerobic Heterotrophic Bacterioplankton in a Meromictic Salt Lake." Applied and Environmental Microbiology 62 (9). https://doi.org/10.1128/aem.62.9.3251-3258.1996.

9. Overmann, J., Hall, K.J., Northcote, T.G., and Beatty J.T. 1999. "Grazing of the Copepod Diaptomus Connexus on Purple Sulphur Bacteria in a Meromictic Salt Lake." Environmental Microbiology 1 (3). https://doi.org/10.1046/j.1462-2920.1999.00026.x.

10. Drews, G. 1985. "Structure and Functional Organization of Light-Harvesting Complexes and Photochemical Reaction Centers in Membranes of Phototrophic Bacteria." Microbiological Reviews, March. https://doi.org/10.1128/mr.49.1.59-70.1985.

11. Parkes-Loach, P.S., Michalski, T.J., Bass, W.J., Smith, U., and Loach, P.A. 1990. "Probing the Bacteriochlorophyll Binding Site by Reconstitution of the Light-Harvesting Complex of Rhodospirillum Rubrum with Bacteriochlorophyll a Analogues." Biochemistry 29 (12). https://doi.org/10.1021/bi00464a010.

12. Sturgis, J.N., and Robert, B. 1996. "The Role of Chromophore Coupling in Tuning the Spectral Properties of Peripheral Light-Harvesting Protein of Purple Bacteria." Photosynthesis Research 50 (1): 5–10. https://doi.org/10.1007/BF00018216.

13. Scheer, H., Svec, W.A., Cope, B.T., Studier, M.H., Scott, R.G., and Katz, J.J. 2002. "Structure of Bacteriochlorophyll b." ACS Publications. American Chemical Society. World. May 1, 2002. https://doi.org/10.1021/ja00818a092.

14. Hashimoto, H., Fujii, R., Yanagi, K., Kusumoto, T., Gardiner, A.T., Cogdell, R.J., *et al.* 2006. "Structures and Functions of Carotenoids Bound to Reaction Centers from Purple Photosynthetic Bacteria." Pure and Applied Chemistry 78 (8): 1505–18. https://doi.org/10.1351/pac200678081505.

15. Turro, N., Ramamurthy, V., and Scaiano, J. 2008. "Principles of Molecular Photochemistry: An Introduction." University Science Books, Mill Valley.

16. Hunter, N.C., Daldal, F., Thurnauer, M.C., Beatty, J.T. (Eds.) 2009 "The Purple Phototrophic Bacteria." Springer, Dordrecht. https://link.springer.com/book/10.1007/978-1-4020-8815-5.

17. Ostroumov, E.E., Mulvaney, R.M., Anna, J.M., Cogdell, R.J. and Scholes, G.D. 2013. "Energy Transfer Pathways in Light-Harvesting Complexes of Purple Bacteria as Revealed by Global Kinetic Analysis of Two-Dimensional Transient Spectra." Research-article. ACS Publications. American Chemical Society. World. July 18, 2013. https://doi.org/10.1021/jp403028x.

18. Weissgerber, T., Zigann, R., Bruce, D., Chang, Y.J., Detter, J.C., Loren Hauser, C.H., *et al.* 2011. "Complete Genome Sequence of Allochromatium Vinosum DSM 180T." Standards in Genomic Sciences 5 (3): 311. https://doi.org/10.4056/sigs.2335270.

19. Nagashima, S., Shimada, K., Matsuura, K., and Nagashima, K.V.P. 2002. "Transcription of Three Sets of Genes Coding for the Core Light-Harvesting Proteins in the Purple Sulfur Bacterium, Allochromatium Vinosum." Photosynthesis Research 74 (3): 269–80. https://doi.org/10.1023/A:1021280104053.

20. Niedzwiedzki, D.M., Bina, D., Picken, N., Honkanen, S.,Blankenship, R.E., Holten, D., Cogdell, R.J. 2012 "Spectroscopic Studies of Two Spectral Variants of Light-Harvesting Complex 2 (LH2) from the Photosynthetic Purple Sulfur Bacterium Allochromatium Vinosum." Biochimica et Biophysica Acta (BBA) - Bioenergetics 1817 (9): 1576–87. https://doi.org/10.1016/j.bbabio.2012.05.009.

21. Frigaard, N.U., Dahl, C. 2009. 'Sulfur Metabolism in Phototrophic Sulfur Bacteria. Advances in Microbial Physiology 54: 103-200.

22. Reinartz, M., Tschäpe, J., Brüser, T., Trüper, H.G., and Dahl, C. 1998. "Sulfide Oxidation in the Phototrophic Sulfur Bacterium Chromatium Vinosum." Archives of Microbiology 170 (1). https://doi.org/10.1007/s002030050615.

23. Gregersen, L.H., Bryant, D.A., and Frigaard, N.U. 2011. "Mechanisms and Evolution of Oxidative Sulfur Metabolism in Green Sulfur Bacteria." Frontiers in Microbiology 2 (May). https://doi.org/10.3389/fmicb.2011.00116.

24. Liu, L.J., Stockdreher, Y., Koch, T., Sun, S.T., Fan, Z., Josten, J., *et al.* 2014. "Thiosulfate Transfer Mediated by DsrE/TusA Homologs from Acidothermophilic Sulfur-Oxidizing Archaeon Metallosphaera Cuprina." Journal of Biological Chemistry 289 (39): 26949–59. https://doi.org/10.1074/jbc.M114.591669.

25. Stockdreher, Y., Sturm, M., Josten, M., Sahl, H.G., Dobler, N., Zigann, R., and Dahl, C. 2014. "New Proteins Involved in Sulfur Trafficking in the Cytoplasm of Allochromatium Vinosum." Journal of Biological Chemistry 289 (18): 12390–403. https://doi.org/10.1074/jbc.M113.536425.

26. Dahl, C. 2015. "Cytoplasmic Sulfur Trafficking in Sulfur-Oxidizing Prokaryotes." IUBMB Life 67 (4): 268–74. https://doi.org/10.1002/iub.1371.

27. Koch, T., and Dahl, C. 2018. "A Novel Bacterial Sulfur Oxidation Pathway Provides a New Link between the Cycles of Organic and Inorganic Sulfur Compounds." The ISME Journal 12 (10): 2479–91. https://doi.org/10.1038/s41396-018-0209-7.

28. Dahl, C. 2017. "Sulfur Metabolism in Phototrophic Bacteria." In Modern Topics in the Phototrophic Prokaryotes, edited by Patrick C. Hallenbeck, 27–66. Cham: Springer International Publishing. https://doi.org/10.1007/978-3-319-51365-2_2.

29. Franz, B., Gehrke T., Lichtenberg H., Hormes J., Dahl C., and Prange A. 2009. "Unexpected Extracellular and Intracellular Sulfur Species during Growth of Allochromatium Vinosum with Reduced Sulfur Compounds." Microbiology (Reading, England) 155 (Pt 8). https://doi.org/10.1099/mic.0.027904-0.

30. Franz, B., Lichtenberg, H., Hormes, J., Modrow, H., Dahl, C., and Prange, A. 2007. "Utilization of Solid 'Elemental' Sulfur by the Phototrophic Purple Sulfur Bacterium Allochromatium Vinosum: A Sulfur K-Edge X-Ray Absorption Spectroscopy Study." Microbiology 153 (4): 1268–74. https://doi.org/10.1099/mic.0.2006/003954-0.

31. Pott, A.S., and Dahl, C. 1998. "Sirohaem Sulfite Reductase and Other Proteins Encoded by Genes at the Dsr Locus of Chromatium Vinosum Are Involved in the Oxidation of Intracellular Sulfur." Microbiology 144 (7): 1881–94. https://doi.org/10.1099/00221287-144-7-1881.

32. Dahl, C., Engels S, Pott-Sperling As, Schulte A, Sander J, Lübbe Y, Deuster O, and Brune Dc. 2005. "Novel Genes of the Dsr Gene Cluster and Evidence for Close Interaction of Dsr Proteins during Sulfur Oxidation in the Phototrophic Sulfur Bacterium Allochromatium Vinosum." Journal of Bacteriology 187 (4). https://doi.org/10.1128/JB.187.4.1392-1404.2005.

33. Sander, J., Engels-Schwarzlose, S.,and Dahl, C. 2006. "Importance of the DsrMKJOP Complex for Sulfur Oxidation in Allochromatium Vinosum and Phylogenetic Analysis of Related Complexes in Other Prokaryotes." Archives of Microbiology 186 (5): 357–66. https://doi.org/10.1007/s00203-006-0156-y.

34. Lübbe, Y.J., Youn, H.S., Timkovich, R., and Dahl, C. 2006. "Siro(Haem)Amide in Allochromatium Vinosum and Relevance of DsrL and DsrN, a Homolog of Cobyrinic Acid a,c-Diamide Synthase, for Sulphur Oxidation." FEMS Microbiology Letters 261 (2): 194–202. https://doi.org/10.1111/j.1574-6968.2006.00343.x.

35. Poulton, S.W., Canfield, D.E. 2011. "Ferruginous Conditions: A Dominant Feature of the Ocean through Earth's History." Elements 7: 107–112.

36. Sperling, E.A., Wolock, C.J., Morgan, A.S., Gill, B.C., Kunzmann, M, Halverson, G.P., Macdonald, F.A., Knoll, A.H., Johnston, D.T. 2015. "Statistical Analysis of Iron Geochemical Data Suggests Limited Late Proterozoic Oxygenation." Nature 523: 451–454.

37. Guilbaud, R., Poulton, S.W., Butterfield, N.J., Zhu, M., Shields-Zhou, G.A. 2015. "A Global Transition to Ferruginous Conditions in the Early Neoproterozoic Oceans." Nature Geoscience 8: 466–470.

38. Canfield, D.E., Zhang, S., Wang, H., Wang, X., Zhao, W., Su, J., Bjerrum, C.J., Haxen, E.R., Hammarlund, E.U. 2018. "A Mesoproterozoic iron formation." Proceedings of National Academy of Science USA 115: 4-51.

39. Motelica-Heino, M., Naylor, C., Zhang, H., Davison, W. 2003. "Simultaneous Release of Metals and Sulfide in Lacustrine Sediment." Environmental Science & Technology 37: 4374-4381.

40. Guo, W., Huo, S.L., Xi, B.D., Zhang, J.T., Wu, F.C. 2015. "Heavy Metal Contamination in Sediments from Typical Lakes in the Five Geographic Regions of China: Distribution, Bioavailability, and Risk." Ecological Engineering 81: 243-255.

41. Tsuji, J.M., Tran, N., Schiff, S.L., Venkiteswaran, J.J., Molot, L.A., Tank, M., Hanada, S., Neufeld, J.D. 2020. "Anoxygenic Photosynthesis and Iron–Sulfur Metabolic Potential of Chlorobia Populations from Seasonally Anoxic Boreal Shield Lakes." The ISME Journal 14: 2732–2747.

42. Skei, J.M., Loring, D.H., Rantala, R.T.T. 1996. "Trace Metals in Suspended Particulate Matter and in Sediment Trap Material from a Permanently Anoxic Fjord- Framvaren, South Norway." Aquatic Geochemistry 2: 131-147.

43. Saulnier, I., Mucci, A. 2000. "Trace Metal Remobilization Following the Resuspension of Estuarine Sediments: Saguenay Fjord, Canada." Appl Geochem 15: 191-210.

44. Gianni, A., Zamparas, M., Papadas, I.T., Kehayias, G., Deligiannakis, Y., Zacharias, L. 2013. "Monitoring and Modeling of Metal Concentration Distributions in Anoxic Basins: Aitoliko Lagoon, Greece." Aquatic Geochemistry 19: 77-95.

45. van der Berg, G.A., Loch, P.G., Winkels, H.J. 1998. "Effects of Fluctuating Hydrological Conditions on the Mobility of Heavy Metals in Soils of a Freshwater Estuary in the Netherlands." Water, Air, and Soil Pollution 102: 377-388.

46. Du Laing, G., Rinklebe, J., Vandecasteele, B., Meers, E., Tack, F.M.G. 2009. "Trace Metal Behavior in Estuarine and Riverine Floodplain Soils and Sediments: A Review." Science of Total Environment 407: 3972-3985.

47. Jian, K.T., Wen, L.S. 2009. "Intra-Annual Variability of Distribution Patterns and Fluxes of Dissolved Trace Metals in a Subtropical Estuary (Danshuei River, Taiwan)." Journal of Marine Systems 75: 87-99.

48. Rona, P.A. 2008. "The Changing Vision of Marine Minerals." Ore Geology Rev 33: 618-666.

49. Scholz, F., McManus, J., Sommer, S. 2013. "The Manganese and Iron Shuttle in a Modern Euxinic Basin and Implications for Molybdenum Cycling at Euxinic Ocean Margins." Chemical Geology 355: 56-68.

50. Riedinger, N., Brunner, B., Krastel, S., Arnold, G.L., Wehrmann, L.M., Formolo, M.J., Beck, A., Bates, S.M., Henkel, S., Lyons, T.W. 2017. "Sulfur Cycling in an Iron Oxide-Dominated, Dynamic Marine Depositional System: the Argentine Continental Margin." Front Earth Sci 5: 33.

51. Picard, A., Gartman, A., Clarke, D.R., Girguis, P.R. 2018. "Sulfate-Reducing Bacteria Influence the Nucleation and Growth of Mackinawite and Greigite." Geochimica et Cosmochimica Acta 220 (1): 367-384. https://doi.org/10.1016/j.gca.2017.10.006.

52. Moreno Flores, E.A. 2019. "Precipitation and Transformation of Iron-Sulfide Nanoparticles in Low-Temperature Aqueous Environment: Effects of Reactant Iron and Sulfide Sources". Open Access Theses & Dissertations 123. https://scholarworks.utep.edu/open_etd/123.

53. Mansor, M., Berti, D., Hochella Jr., M. F., Murayama, M. and Xu, J. 2019. "Phase, morphology, elemental composition, and formation mechanisms of biogenic and abiogenic Fe-Cu-sulfide nanoparticles: A comparative study on their occurrences under anoxic conditions." American Mineralogist 104 (5): 703-717. https://doi.org/10.2138/am-2019-6848.

54. Mansor, M., Winkler, C., Hochella Jr., M. F., Xu, J. 2019. "Nanoparticulate Nickel-Hosting Phases in Sulfidic Environments: Effects of Ferrous Iron and Bacterial Presence on Mineral Formation Mechanism and Solid-Phase Nickel Distribution." Frontiers in Earth Science 7. https://doi.org/10.3389/feart.2019.00151.

55. Mansor, M., Cantando, E., Wang, Y., Hernandez-Viezcas, J.A., Gardea-Torresdey, J.L., Hochella Jr., M.F., Xu, J. 2020. "Insights into the Biogeochemical Cycling of Cobalt: Precipitation and Transformation of Cobalt Sulfide Nanoparticles under Low-Temperature Aqueous Conditions." Environmental Science & Technology 54 (9): 5598-5607. https://doi.org/10.1021/acs.est.0c01363.

56. Bolger, A.M., Lohse, M., and Usadel, B. 2014. "Trimmomatic: a flexible trimmer for illumina sequence data." Bioinformatics 30: 2114–20.

889 57. Langmead, B., and Salzberg, S.L. 2012. "Fast gapped-read alignment with Bowtie 2." Nature
890 methods 9.4: 357-359.

891 58. Love, M.I., Huber, W., Anders, S. 2014. "Moderated estimation of fold change and
892 dispersion for RNA-seq data with DESeq2." Genome Biology 15 (550). doi:10.1186/s13059-
893 014-0550-8.

894 59. Weissgerber, T., Dobler, N., Polen, T., Latus, J., Stockdreher, Y., and Dahl, C. 2013.
895 "Genome-Wide Transcriptional Profiling of the Purple Sulfur Bacterium Allochromatium
896 Vinosum DSM 180T during Growth on Different Reduced Sulfur Compounds." Journal of
897 Bacteriology 195 (18): 4231–45. https://doi.org/10.1128/JB.00154-13.

898 60. Shi, L., Dong, H., Reguera, G., Beyenal, H., Lu, A., Liu, J., Yu, H.Q., and Fredrickson, J.K.
899 2016. "Extracellular Electron Transfer Mechanisms between Microorganisms and Minerals."
900 Nature Reviews Microbiology 14 (10): 651–62. https://doi.org/10.1038/nrmicro.2016.93.

901 61. Breuer, M., Rosso, K.M., Blumberger, J., and Butt, J.N. 2015. "Multi-Haem Cytochromes in
902 Shewanella Oneidensis MR-1: Structures, Functions and Opportunities." Journal of the Royal
903 Society, Interface 12 (102). https://doi.org/10.1098/rsif.2014.1117.

904 62. Chong, G.W., Karbelkar, A.A., and El-Naggar, M.Y. 2018. "Nature's Conductors: What Can
905 Microbial Multi-Heme Cytochromes Teach Us about Electron Transport and Biological Energy
906 Conversion?" Current Opinion in Chemical Biology 47 (December): 7–17.
907 https://doi.org/10.1016/j.cbpa.2018.06.007.

908 63. Costa, N.L., Clarke, T.A., Philipp, L.A., Gescher, J., Louro, R.O., Paquete, C.M. 2018.
909 "Electron Transfer Process in Microbial Electrochemical Technologies: The Role of Cell-Surface
910 Exposed Conductive Proteins." Bioresource Technology 258: (May): 308-317.
911 https://doi.org/10.1016/j.biortech.2018.01.133.

912 64. Gray, H., and Winkler, J. 2003. "Electron Tunneling through Proteins." Quarterly Reviews of
913 Biophysics 36(3): 341-372. doi:10.1017/S0033583503003913

914 65. Myers, C.R., and Myers, J.M. 2004. "The Outer Membrane Cytochromes of *Shewanella*
915 *oneidensis* MR-1 are Lipoproteins." Letters in Applied Microbiology 39: 466–470.

916 66. Teufel, F., Armenteros, J.J.A, Johansen, A.R., Gíslason, M.H., Pihl, S.I., Tsirigos, K.D.,
917 Winther, O., Brunak, S., Heijne, G., and Nielsen, H. 2022. "SignalP 6.0 Predicts All Five Types
918 of Signal Peptides Using Protein Language Models." Nature Biotechnology 40 (7): 1023–25.
919 https://doi.org/10.1038/s41587-021-01156-3.

920 67. Viale, A., Kobayashi H., Akazawa T. 1989. "Expressed Genes for Plant-Type Ribulose 1,5-
921 Bisphosphate Carboxylase/Oxygenase in the Photosynthetic Bacterium Chromatium Vinosum,
922 Which Possesses Two Complete Sets of the Genes." Journal of Bacteriology 171 (5).
923 https://doi.org/10.1128/jb.171.5.2391-2400.1989.

924 68. Hayashi, N.R., Arai, H., Kodama, T., and Igarashi, Y. 1999. "The CbbQ Genes, Located
925 Downstream of the Form I and Form II RubisCO Genes, Affect the Activity of Both RubisCOs."

Biochemical and Biophysical Research Communications 265 (1). https://doi.org/10.1006/bbrc.1999.1103.

69. Badger, M.R., and Bek, E.J. 2008. "Multiple Rubisco Forms in Proteobacteria: Their Functional Significance in Relation to CO2 Acquisition by the CBB Cycle." Journal of Experimental Botany 59 (7): 1525–41. https://doi.org/10.1093/jxb/erm297.

70. Hanson, T.E., and Tabita, F.R. 2001. "A Ribulose-1,5-Bisphosphate Carboxylase/Oxygenase (RubisCO)-like Protein from Chlorobium Tepidum That Is Involved with Sulfur Metabolism and the Response to Oxidative Stress." Proceedings of the National Academy of Sciences 98 (8): 4397–4402. https://doi.org/10.1073/pnas.081610398.

71. Hanson, T.E., and Tabita F.R. 2003. "Insights into the Stress Response and Sulfur Metabolism Revealed by Proteome Analysis of a Chlorobium Tepidum Mutant Lacking the Rubisco-like Protein." Photosynthesis Research 78 (3). https://doi.org/10.1023/B:PRES.0000006829.41444.3d.

72. Chen, Z.W., Koh, M., Van Driessche, G., Van Beeumen, J.J., Bartsch, R.G., Meyer, T.E., Cusanovich, M.A., and Mathews, F.S. 1994. "The Structure of Flavocytochrome *c* Sulfide Dehydrogenase from a Purple Phototrophic Bacterium." Science 266 (5184): 430–32. https://doi.org/10.1126/science.7939681.

73. Walsh, C.T. 2020 "The Chemical Biology of Sulfur." United Kingdom: Royal Society of Chemistry, 2020.

74. Griesbeck, C., Schütz, M., Schödl, T., Bathe, S., Nausch, L., Mederer, L., Vielreicher, M., and Hauska, S. 2002. "Mechanism of Sulfide-Quinone Reductase Investigated Using Site-Directed Mutagenesis and Sulfur Analysis." Research-article. ACS Publications. American Chemical Society. World. September 7, 2002. https://doi.org/10.1021/bi026032b.

75. Pattaragulwanit, K., Brune, D.C., Trüper, H.G., and Dahl, C. 1998. "Molecular Genetic Evidence for Extracytoplasmic Localization of Sulfur Globules in Chromatium Vinosum." Archives of Microbiology 169 (5): 434–44. https://doi.org/10.1007/s002030050594.

76. Prange, A., Engelhardt, H., Trüper, H.G., and Dahl, C. 2004. "The Role of the Sulfur Globule Proteins of Allochromatium Vinosum: Mutagenesis of the Sulfur Globule Protein Genes and Expression Studies by Real-Time RT-PCR." Archives of Microbiology 182 (2): 165–74. https://doi.org/10.1007/s00203-004-0683-3.

77. Grein, F., Pereira, I.A.C., Dahl, C. 2010. "Biochemical Characterization of Individual Components of the *Allochromatium vinosum* DsrMKJOP Transmembrane Complex Aids Understanding of Complex Function In Vivo." Journal of Bacteriology 192 (24). https://doi.org/10.1128/JB.00849-10.

78. Grimm, F., Dobler, N., and Dahl, C. 2010. "Regulation of Dsr Genes Encoding Proteins Responsible for the Oxidation of Stored Sulfur in Allochromatium Vinosum." Microbiology 156 (3): 764–73. https://doi.org/10.1099/mic.0.034645-0.

79. Armitage, J.P. 2009. “Swimming and Behavior in Purple Non-Sulfur Bacteria.” In The Purple Phototrophic Bacteria, 643–54. Springer, Dordrecht. https://doi.org/10.1007/978-1-4020-8815-5_32.

80. Guiral, M., Prunetti, L., Aussignargues, C., Ciaccafava, A., Infossi, P., Ilbert, M., Lojou, E., *et al.* 2012 “The Hyperthermophilic Bacterium Aquifex Aeolicus: From Respiratory Pathways to Extremely Resistant Enzymes and Biotechnological Applications.” In Advances in Microbial Physiology, 61:125–94. Academic Press. https://doi.org/10.1016/B978-0-12-394423-8.00004-4.

81. Xu, Y., Schoonen, Martin A. A. 2000. "The absolute energy positions of conduction and valence bands of selected semiconducting minerals" *American Mineralogist*, 85: 543-556. https://doi.org/10.2138/am-2000-0416

82. Blankenship, R.E. 2010. “Early Evolution of Photosynthesis.” Future Perspectives in Plant Biology. http://www.plantphysiol.org/content/154/2/434.full

83. Zhang, Q., Ma, W., Peng, Q., Shu, X. 2020. “Stabilization and Utilization of Pyrite under Light Irradiation: Discussion of Photocorrosion Resistance.” ACS Omega, 5: 28693−28701

Table 1. Compilation of top differentially regulated genes for *A vinosum* when grown on pyrite versus dissolved sulfide. The genes without a designated annotation are highlighted in gray. (The complete data are in supplemental Table 52)

No.	*Gene locus*	*log2FC*	P_{adj}	*KEGG or Strindb annotation*
Upregulated genes				
1	Alvin 1093	7.45	5.6E-132	Diheme cytochrome subunit of sulfide dehydrogenase
2	Alvin 0022	7.10	7.8E-116	Domain of unknown function DUF1924
3	Alvin 1092	6.18	1.7E-75	Flavocytochrome c sulphide dehydrogenase
4	Alvin 0023	5.54	1.8E-85	Diheme cytochrome c
5	Alvin 1379	5.50	1.9E-03	2-isopropylmalate synthase
6	Alvin 1095	5.39	2.1E-87	epoxyqueuosine reductase
7	Alvin 0024	5.32	8.9E-30	membrane protein-like protein
8	Alvin 0021	5.13	4.6E-46	cytochrome B561
9	Alvin 1094	4.83	4.2E-62	uncharacterized protein
10	Alvin 0013	4.59	3.0E-36	outer membrane efflux protein
11	Alvin 2309	4.57	2.1E-52	Hydrogenase (NiFe) small subunit HydA
12	Alvin 2308	4.50	7.3E-64	Hydrogenase (NiFe) small subunit HydA
13	Alvin 0020	4.38	1.0E-37	Diheme cytochrome c
15	Alvin 0014	4.21	1.1E-29	efflux transporter, RND family, MFP subunit
16	Alvin 0025	4.15	3.8E-35	two component transcriptional regulator
18	Alvin 2307	3.90	1.9E-70	Ni/Fe-hydrogenase, b-type cytochrome subunit
21	Alvin 2451	3.63	2.7E-37	molybdopterin oxidoreductase Fe454 region
22	Alvin 1527	3.62	7.3E-26	FeoA family protein (Fe2+ transport)
23	Alvin 0019	3.51	2.4E-26	ferrous-iron efflux pump FieF
26	Alvin 1848	3.51	1.1E-35	isocitrate lyase
27	Alvin 2446	3.44	7.5E-17	nitrite and sulphite reductase 4Fe-45 region
29	Alvin 1878	3.36	2.6E-03	nitrogen fixation protein FixT
30	Alvin 0017	3.36	5.6E-29	XRE family transcriptional regulator
31	Alvin 2306	3.29	4.8E-36	hydrogenase expression/formation protein, HoxM
32	Alvin 0018	3.24	4.1E-26	Di-heme cytochrome c peroxidase
33	Alvin 3291	3.20	4.8E-30	hypothetical protein
34	Alvin 1145	3.09	1.9E-39	periplasmic protein CpxP/5py
35	Alvin 0015	3.02	9.0E-19	heavy metal efflux pump, CzcA family
36	Alvin 2447	3.00	4.2E-12	adenylylsulfate reductase
37	Alvin 2093	2.96	9.6E-11	hydrogenase (NiFe) small subunit HydA
38	Alvin 0016	2.93	3.2E-15	conserved hypothetical protein
39	Alvin 2111	2.92	1.9E-41	5ulfur-oxidizing protein 5oxY
40	Alvin 3196	2.81	3.3E-07	hypothetical protein
41	Alvin 0431	2.81	1.9E-17	hypothetical protein

42	Alvin 1034	2.77	3.5E-19	Phosphoketolase
43	Alvin 3016	2.75	2.7E-19	type IV fimbrial biogenesis protein FimT
44	Alvin 0929	2.75	4.8E-13	hypothetical protein
45	Alvin 0926	2.61	9.7E-15	PRC-barrel domain protein
46	Alvin 2452	2.57	2.1E-19	formate dehydrogenase, alpha subunit
47	Alvin 2092	2.50	3.3E-13	conserved hypothetical protein
48	Alvin 2110	2.50	3.3E-12	peptidase M48 5te24p
49	Alvin 1143	2.47	1.4E-15	twin-arginine translocation pathway signal
50	Alvin 1556	2.46	5.9E-31	hypothetical protein
51	Alvin 3275	2.44	2.9E-19	phage recombination protein Bet
52	Alvin 1525	2.43	1.1E-17	ferrous iron transport protein B
53	Alvin 2112	2.40	2.4E-21	5oxZ; PFAM: 5ulphur oxidation protein 5oxZ
54	Alvin 1420	2.39	1.9E-26	iron-sulfur cluster assembly transcription factor IscR
55	Alvin 1524	2.30	2.3E-03	Protein of unknown function DUF1920
56	Alvin 0483	2.29	2.8E-20	catalase/peroxidase HPI
57	Alvin 1152	2.26	3.8E-20	uncharacterized conserved protein UCP029693
58	Alvin 2311	2.26	5.9E-16	transaldolase
59	Alvin 1146	2.24	4.4E-19	hypothetical protein
60	Alvin 1446	2.22	2.7E-12	antitoxin HigA-1
61	Alvin 2710	2.22	2.6E-06	hypothetical protein
62	Alvin 1954	2.21	1.2E-14	flagellar protein Fli5
63	Alvin 1856	2.20	5.6E-16	Fe(ii) trafficking protein yggx;
64	Alvin 1521	2.19	2.3E-15	Cu(i)/ag(i) efflux system periplasmic protein cusf;
65	Alvin 0492	2.18	6.2E-19	conserved hypothetical protein
66	Alvin 2145	2.18	6.9E-16	sulfide:quinone oxidoreductase
67	Alvin 0026	2.18	1.5E-14	Integral membrane signal transduction histidine kinase
68	Alvin 0900	2.17	2.1E-14	hypothetical protein
69	Alvin 2989	2.17	2.8E-18	NAD(P)H dehydrogenase (quinone)
70	Alvin 1144	2.15	3.9E-07	CsbD family protein
71	Alvin 1953	2.15	6.9E-25	flagellar hook-associated 2 domain protein
72	Alvin 1150	2.12	9.5E-16	conserved hypothetical protein
73	Alvin 1952	2.07	3.6E-25	flagellar protein FlaG
74	Alvin 2454	2.06	5.3E-11	formate dehydrogenase subunit gamma
75	Alvin 1877	2.05	5.3E-04	4Fe-45 ferredoxin iron-sulfur binding domain protein
76	Alvin 0107	2.05	3.9E-13	conserved hypothetical protein
77	Alvin 2704	2.04	1.1E-12	conserved hypothetical protein
78	Alvin 2312	2.01	1.2E-09	Integral membrane protein TerC (tellurite resistance)
79	Alvin 0098	2.01	2.8E-16	transcriptional regulator, GntR family
80	Alvin 1154	2.00	7.4E-08	conserved hypothetical protein
Downregulated genes				
81	Alvin 0704	-6.85	1.2E-47	Antenna complex alpha/beta subunit
82	Alvin 0703	-6.83	3.3E-10	hypothetical protein
83	Alvin 0705	-6.62	1.5E-78	hypothetical protein

84	Alvin 1741	-6.22	3.7E-36	hypothetical protein
85	Alvin 0706	-6.21	1.4E-42	antenna complex alpha/beta subunit
86	Alvin 0709	-5.80	6.1E-21	Light-harvesting complex 1 beta chain
87	Alvin 0962	-5.75	6.5E-108	uncharacterized protein
88	Alvin 1740	-5.48	4.9E-36	Dinitrogenase iron-molybdenum cofactor biosynthesis protein
89	Alvin 2136	-5.23	9.4E-76	hypothetical protein
90	Alvin 1739	-5.16	1.2E-51	Cobyrinic acid ac-diamide synthase
91	Alvin 1365	-4.74	4.0E-08	Ribulose-bisphosphate carboxylase
92	Alvin 1251	-4.72	2.5E-25	Dissimilatory sulfite reductase alpha subunit
93	Alvin 3072	-4.69	3.2E-68	conserved hypothetical protein
94	Alvin 1252	-4.45	4.8E-30	dissimilatory sulfite reductase beta subunit
95	Alvin 2515	-4.06	9.3E-94	hypothetical protein
96	Alvin 2248	-3.99	8.1E-23	Outer membrane receptor for ferrienterochelin and colicins;
97	Alvin 2497	-3.96	1.7E-52	conserved hypothetical protein
98	Alvin 0747	-3.87	2.6E-18	peptidase C39 bacteriocin processing
99	Alvin 1006	-3.87	3.6E-47	Peroxiredoxin
100	Alvin 2498	-3.59	1.6E-74	nitrogen fixation-related protein
101	Alvin 1253	-3.54	3.2E-26	DsrE
102	Alvin 1367	-3.48	1.3E-03	CbbQ/NirQ/NorQ domain protein
103	Alvin 0707	-3.41	5.2E-20	regulatory protein LuxR
104	Alvin 2767	-3.37	4.1E-51	DEAD/DEAH box helicase domain protein
105	Alvin 1738	-3.35	7.8E-38	Cobyrinic acid ac-diamide synthase
106	Alvin 1711	-3.28	1.8E-08	hypothetical protein
107	Alvin 0500	-3.27	6.8E-27	protein of unknown function DUF150
108	Alvin 1366	-3.25	1.0E-03	Ribulose-bisphosphate carboxylase
109	Alvin 0749	-3.17	5.2E-04	hypothetical protein
110	Alvin 2759	-3.15	8.0E-03	hypothetical protein
111	Alvin 1841	-3.13	1.3E-64	Protein of unknown function
112	Alvin 2550	-3.10	2.2E-11	antenna complex alpha/beta subunit
113	Alvin 2572	-3.07	2.0E-28	RNA polymerase, sigma 32 subunit, RpoH
114	Alvin 3032	-3.04	8.0E-33	conserved hypothetical protein
115	Alvin 0708	-3.03	2.3E-07	hypothetical protein
116	Alvin 1737	-2.98	1.9E-15	Dinitrogenase iron-molybdenum cofactor biosynthesis protein
117	Alvin 2429	-2.95	8.1E-39	NADH-quinone oxidoreductase, B subunit
118	Alvin 1508	-2.92	4.9E-23	sulfur relay protein, TusE/DsrC/DsvC family
119	Alvin 1254	-2.88	1.9E-19	DsrF
120	Alvin 2576	-2.80	1.9E-02	antenna complex alpha/beta subunit
121	Alvin 0501	-2.79	2.6E-22	NusA antitermination factor
122	Alvin 2250	-2.78	1.5E-21	Biopolymer transport protein ExbD/TolR
123	Alvin 2577	-2.78	7.9E-03	antenna complex alpha/beta subunit

124	Alvin 2428	-2.76	1.8E-30	NADH (or F420H2) dehydrogenase, subunit C
125	Alvin 2768	-2.74	2.1E-25	RNP-1 like RNA-binding protein
126	Alvin 1122	-2.73	2.5E-16	conserved hypothetical protein
127	Alvin 2554	-2.73	4.3E-03	antenna complex alpha/beta subunit
128	Alvin 1688	-2.73	1.5E-06	Antibiotic biosynthesis monooxygenase
129	Alvin 2430	-2.73	4.4E-30	NADH-ubiquinone/plastoquinone oxidoreductase chain 3
130	Alvin 3073	-2.70	4.2E-22	C4-dicarboxylate transporter/malic acid transport protein
131	Alvin 0834	-2.69	9.0E-19	NAD(P)(+) transhydrogenase (AB-specific)
132	Alvin 2549	-2.68	1.8E-02	antenna complex alpha/beta subunit
133	Alvin 2249	-2.66	1.1E-26	MotA/TolQ/ExbB proton channel
134	Alvin 2251	-2.65	8.3E-18	Biopolymer transport protein ExbD/TolR
135	Alvin 2551	-2.64	5.0E-03	photosynthetic reaction centre cytochrome c subunit
136	Alvin 2600	-2.63	7.8E-23	5irA family protein
137	Alvin 0744	-2.63	6.5E-11	sigma54 specific transcriptional regulator, Fis family
138	Alvin 2432	-2.62	8.7E-30	triosephosphate isomerase
139	Alvin 0805	-2.60	1.4E-23	2-oxo-acid dehydrogenase E1 subunit, homodimeric type
140	Alvin 2579	-2.59	1.9E-02	antenna complex alpha/beta subunit
141	Alvin 1687	-2.58	6.6E-06	ATP dependent RNA helicase
142	Alvin 2760	-2.57	9.1E-09	antenna complex alpha/beta subunit
143	Alvin 2254	-2.56	2.2E-14	conserved hypothetical protein
144	Alvin 2548	-2.54	7.5E-10	antenna complex alpha/beta subunit
145	Alvin 2552	-2.51	5.5E-03	photosynthetic reaction center, M subunit
146	Alvin 1712	-2.48	2.1E-12	conserved hypothetical protein
147	Alvin 0316	-2.45	2.2E-19	transketolase
148	Alvin 2280	-2.44	1.7E-26	translation initiation factor IF-1
149	Alvin 2599	-2.35	8.7E-23	Rhodanese domain protein
150	Alvin 1690	-2.32	6.1E-13	transport system permease protein
151	Alvin 1754	-2.29	2.9E-13	translation elongation factor P
152	Alvin 1689	-2.28	9.4E-15	periplasmic binding protein
153	Alvin 2484	-2.25	1.5E-17	165 rRNA processing protein RimM
154	Alvin 1483	-2.24	2.9E-13	hydrolase, TatD family
155	Alvin 1890	-2.23	2.1E-15	acyl carrier protein
156	Alvin 0040	-2.20	3.1E-17	ATP synthase F0, A subunit
157	Alvin 2427	-2.20	2.7E-16	NADH dehydrogenase I, D subunit
158	Alvin 1691	-2.19	4.8E-08	ABC transporter related protein
159	Alvin 0499	-2.19	1.2E-14	hypothetical protein
160	Alvin 1259	-2.19	1.7E-18	DsrL
161	Alvin 1753	-2.18	8.6E-22	tRNA synthetase class II
162	Alvin 1893	-2.18	3.3E-09	3-oxoacyl-(acyl-carrier-protein) synthase III
163	Alvin 1258	-2.17	2.9E-26	dsrK
164	Alvin 1896	-2.17	7.0E-19	protein of unknown function DUF177
165	Alvin 3195	-2.16	1.2E-03	hypothetical protein
166	Alvin 0039	-2.16	3.3E-21	ATP synthase I chain

167	Alvin 0804	-2.15	9.7E-26	pyruvate dehydrogenase complex dihydrolipoamide
168	Alvin 0746	-2.15	4.3E-10	hypothetical protein
169	Alvin 0315	-2.14	6.4E-13	glyceraldehyde-3-phosphate dehydrogenase, type I
170	Alvin 1734	-2.12	9.5E-08	Protein of unknown function DUF2269, transmembrane
171	Alvin 1260	-2.11	4.5E-15	dsrJ
172	Alvin 2426	-2.11	2.6E-10	NADH-quinone oxidoreductase, E subunit
173	Alvin 2758	-2.10	7.8E-22	poly(A) polymerase
174	Alvin 2601	-2.09	2.0E-20	conserved hypothetical protein
175	Alvin 2156	-2.08	6.6E-11	GTP-binding protein Obg/CgtA
176	Alvin 2252	-2.07	3.1E-12	TonB family protein
177	Alvin 2491	-2.06	3.8E-19	molybdopterin oxidoreductase
178	Alvin 2602	-2.03	1.6E-19	acetolactate synthase, large subunit
179	Alvin 2415	-2.01	8.4E-09	conserved hypothetical protein
180	Alvin 1644	-2.01	1.4E-14	integration host factor, beta subunit
181	Alvin 1079	-2.01	2.0E-10	cytochrome B561
182	Alvin 2386	-2.00	2.2E-23	peptide chain release factor 1

Table 2. Differential expression of *puf* and *puc* genes in the pyrite-supported *A vinosum* cells. Only those with a P value of < 0.05 are presented.

Gene	Protein	log_2FC	P_{adj}
***puf* genes (LH1)**			
Alvin_2550	puf/LH1	-3.105	2.23E-11
Alvin_2554	puf/LH1	-2.729	0.0042904
Alvin_2549	puf/LH1	-2.685	0.0180326
Alvin_2551	pufC	-2.637	0.0050426
Alvin_2548	puf/LH1	-2.543	7.53E-10
Alvin_2552	pufM	-2.506	0.0054761
Alvin_2555	puf/LH1	-1.963	9.55E-05
Alvin_2553	pufL	-1.657	1.18E-06
Alvin_2634	puf/LH1	-1.571	1.35E-11
***puc* genes (LH2)**			
Alvin_0704	pucB6	-6.853	1.15E-47
Alvin_0703	pucA6	-6.829	3.27E-10
Alvin_0705	pucA5	-6.622	1.51E-78
Alvin_0706	pucB5	-6.214	1.40E-42
Alvin_0709	pucB4	-5.797	6.10E-21
Alvin_2759	pucA3	-3.155	7.98E-03
Alvin_0708	pucA4	-3.027	2.25E-07
Alvin_2576	pucA2	-2.803	1.89E-02
Alvin_2577	pucB2	-2.775	0.0079294
Alvin_2579	pucB1	-2.594	1.93E-02
Alvin_2760	pucB3	-2.570	9.14E-09
Alvin_2578	pucA1	-1.997	0.000097

Table 3. Differential expression of *sax* and *dsr* genes in the pyrited-supported *A. vinasum* cells. Only those with a P value < 0.05 are presented.

Gene	Protein	log_2FC	P_{adj}
***dsr* genes**			
Alvin_1251	DsrA	-4.723	2.54E-25
Alvin_1252	DsrB	-4.454	4.76E-30
Alvin_1253	DsrE	-3.541	3.15E-26
Alvin_1254	DsrF	-2.883	1.89E-19
Alvin_1259	DsrL	-2.187	1.70E-18
Alvin_1258	DsrK	-2.168	2.94E-26
Alvin_1260	DsrJ	-2.113	4.47E-15
Alvin_1261	DsrO	-1.987	5.20E-20
Alvin_1262	DsrP	-1.678	1.86E-15
Alvin_1256	DsrC	-1.247	1.07E-07
***sox* genes**			
Alvin_2111	SoxY	2.919	1.91E-41
Alvin_2112	SoxZ	2.40	2.39E-21
Alvin_2167	SoxB	1.22	2.19E-07
Alvin_2169	SoxA	1.175	0.00714587
Alvin_2168	SoxX	1.074	0.00178113

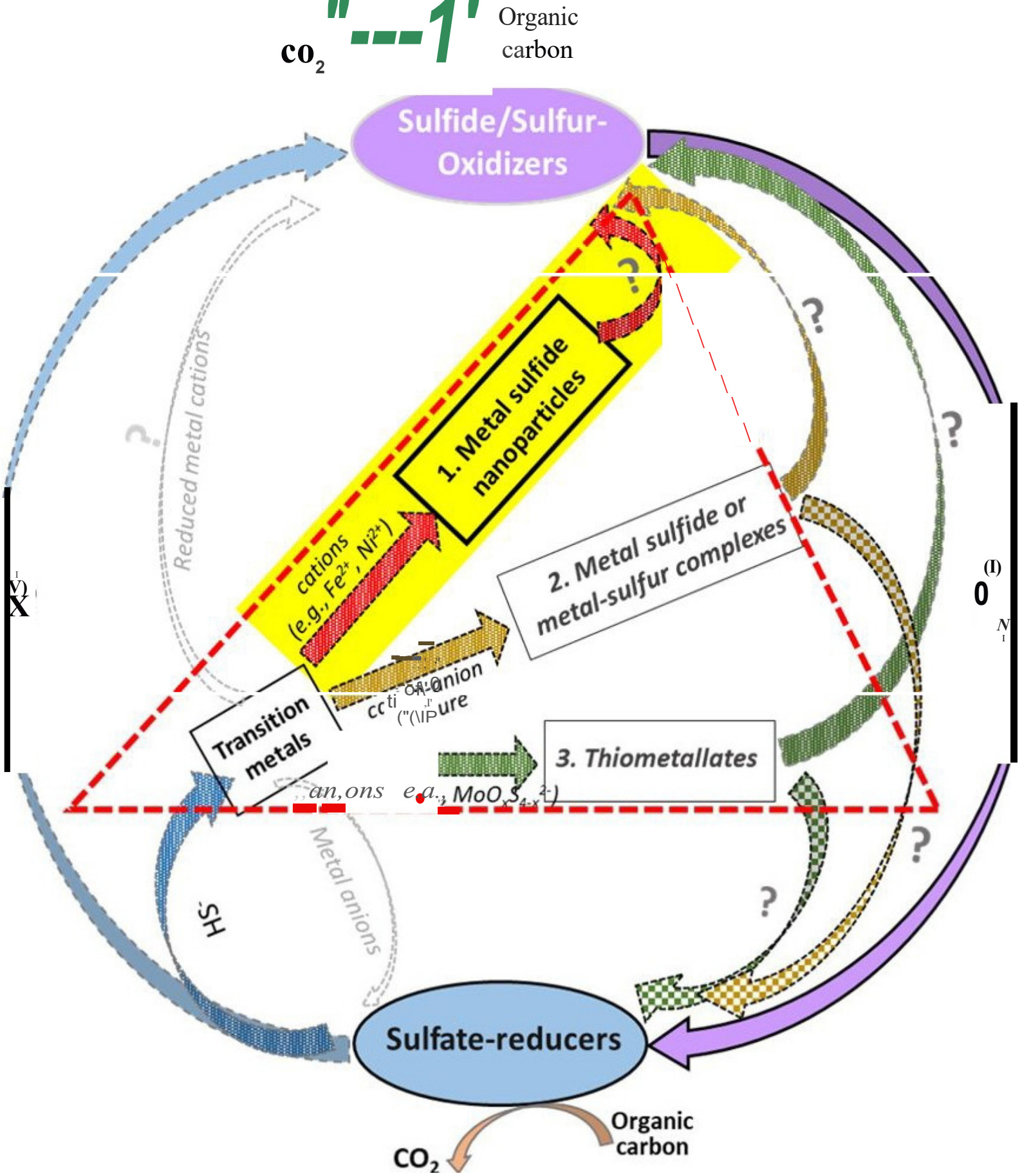
Organic carbon
CO_2
Sulfide/Sulfur-Oxidizers
Reduced metal cations
1. Metal sulfide nanoparticles
cations (e.g., Fe^{2+}, Ni^{2+})
2. Metal sulfide or metal-sulfur complexes
Transition metals
3. Thiometallates
Metal anions
HS^-
Sulfate-reducers
Organic carbon
CO_2

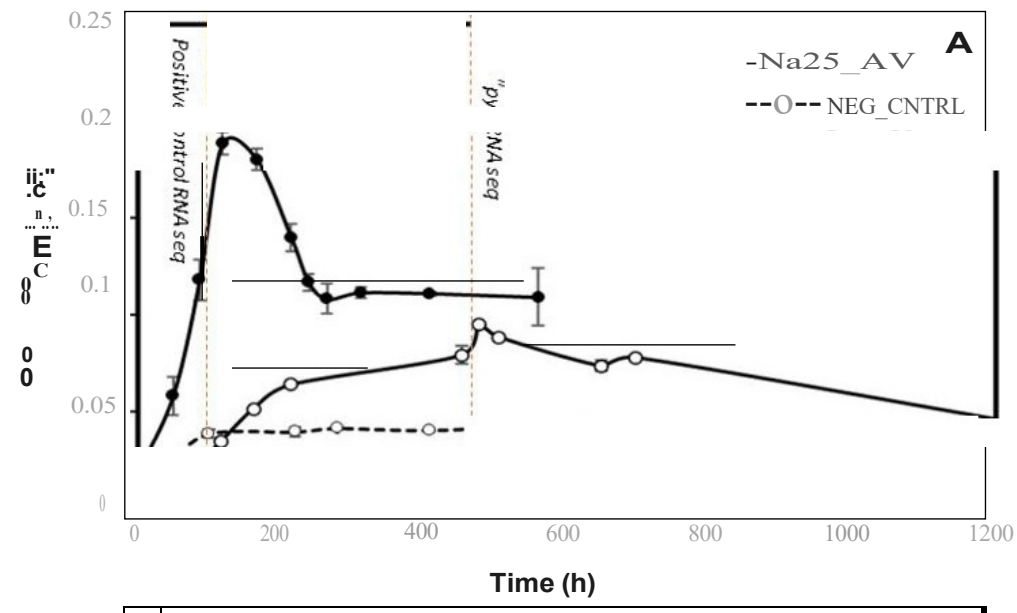
A
-Na25_AV
--0-- NEG_CNTRL
Positive
ntrol RNA seq
py
NA seq
Time (h)

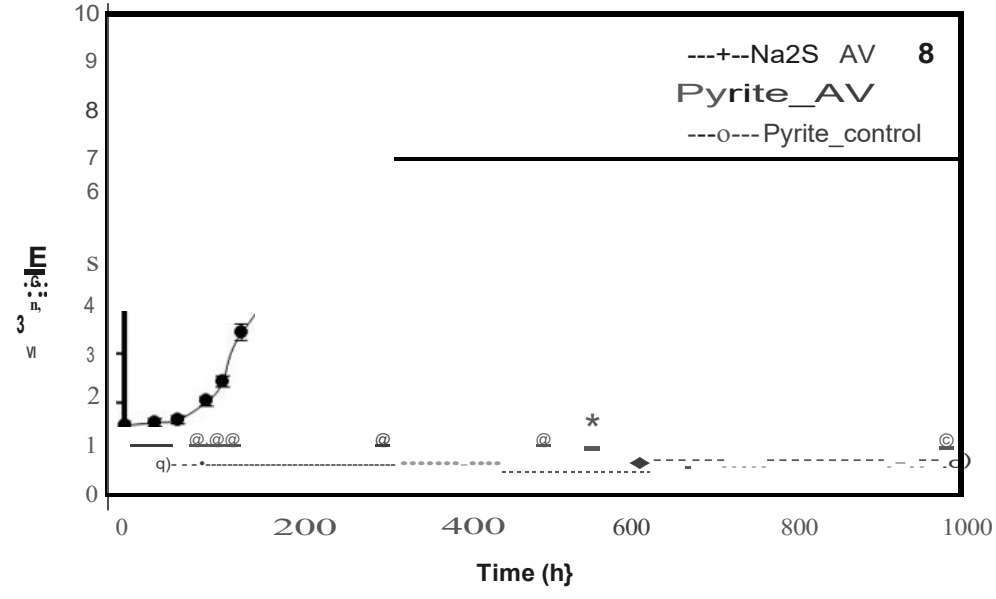
8
---+--Na2S AV
Pyrite_AV
---o--- Pyrite_control
Time (h}

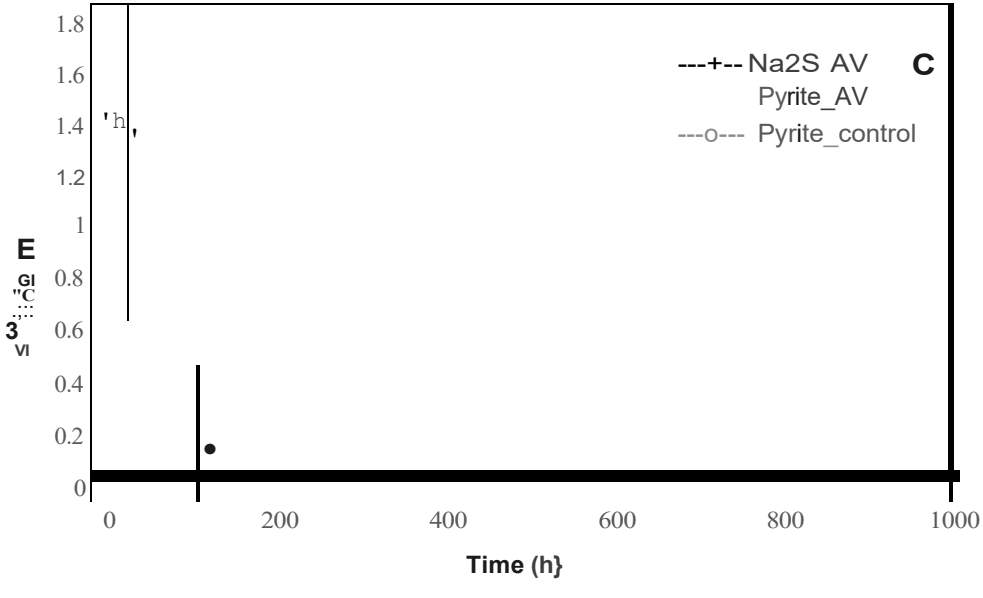
C
---+-- Na2S AV
Pyrite_AV
---o--- Pyrite_control
Time (h}

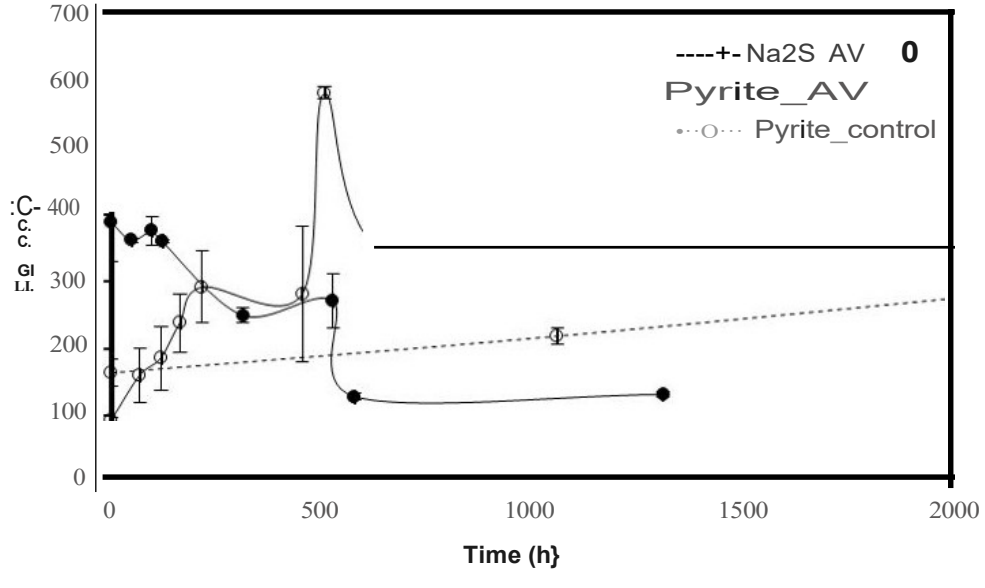
0
----+- Na2S AV
Pyrite_AV
•··o··· Pyrite_control
Time (h}

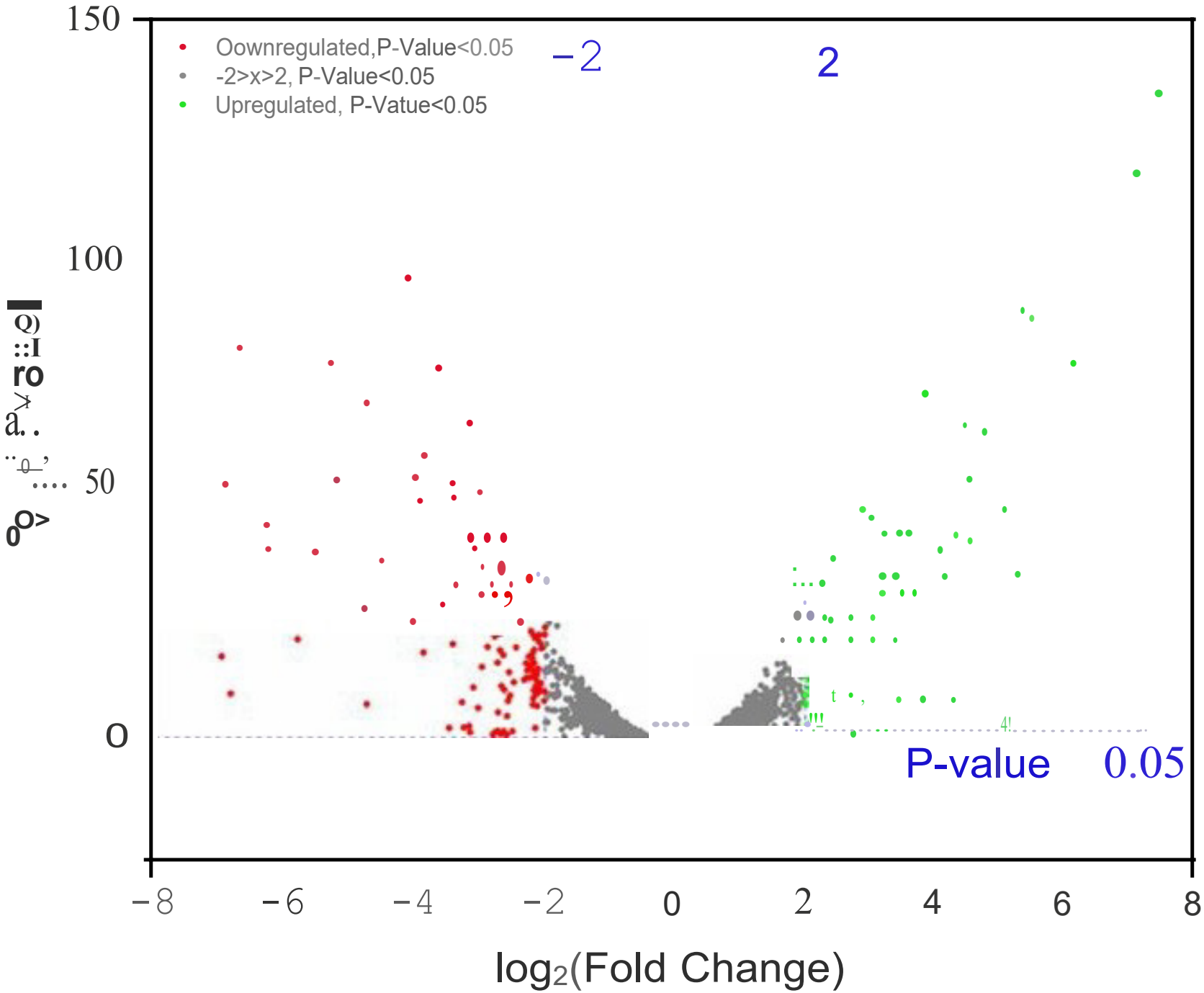
Oownregulated,P-Value<0.05
-2>x>2, P-Value<0.05
Upregulated, P-Vatue<0.05
−2
2
P-value
0.05
150
100
50
0
−8
−6
−4
−2
0
2
4
6
8
log2(Fold Change)

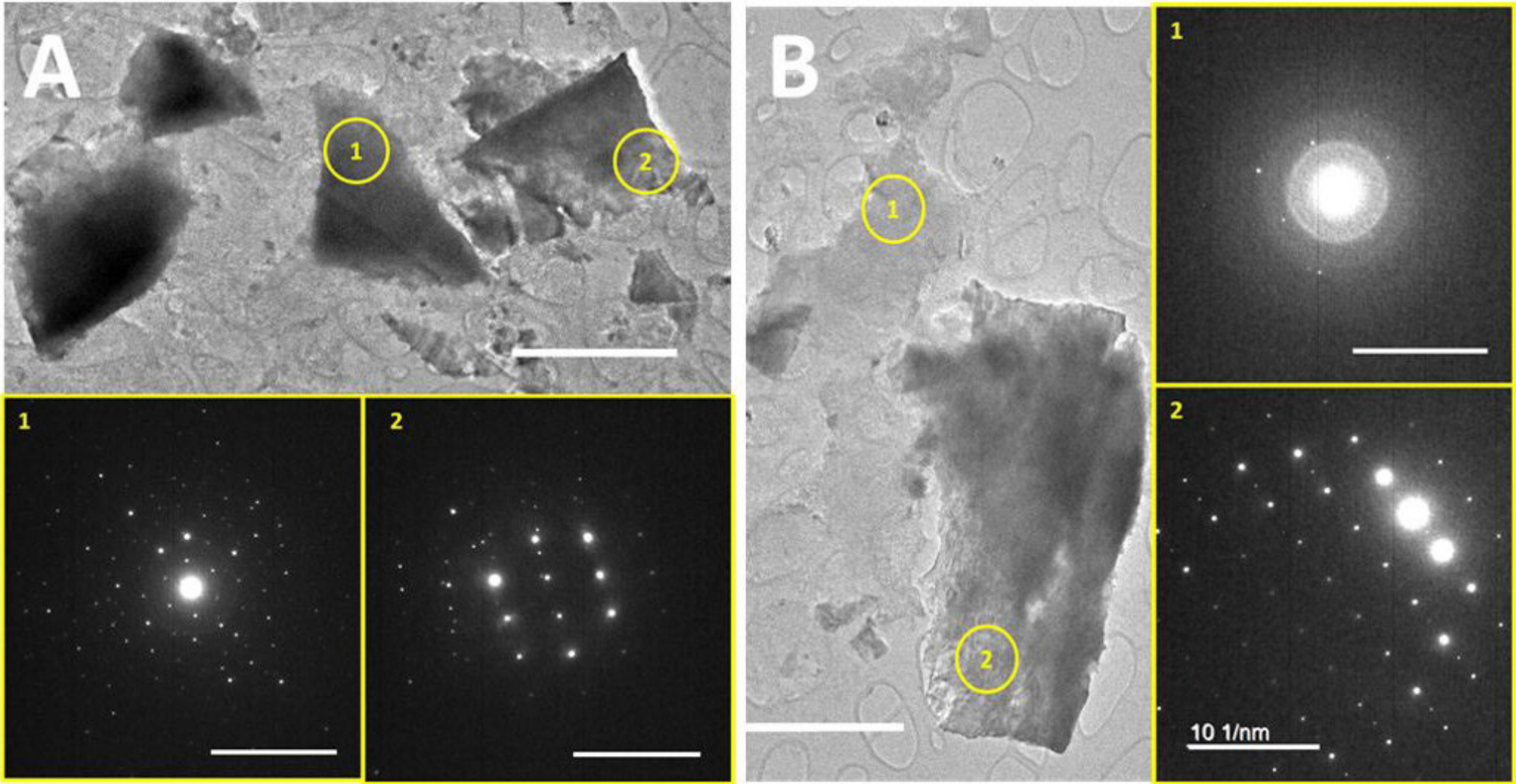
A
1
2
1
2
B
1
2
1
2
10 1/nm

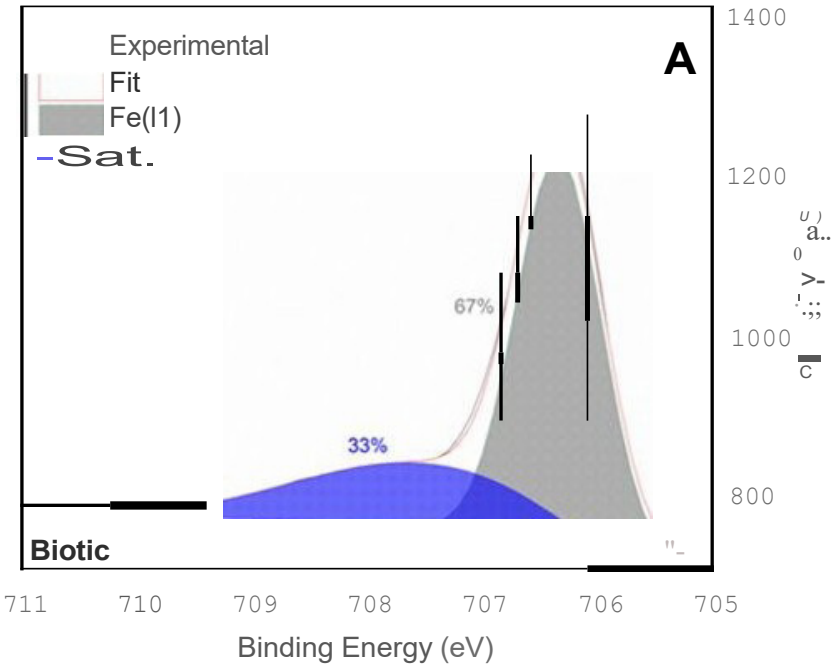
A
Experimental
Fit
Fe(I1)
-Sat.
67%
33%
Biotic
1400
1200
1000
800
711
710
709
708
707
706
705
Binding Energy (eV)

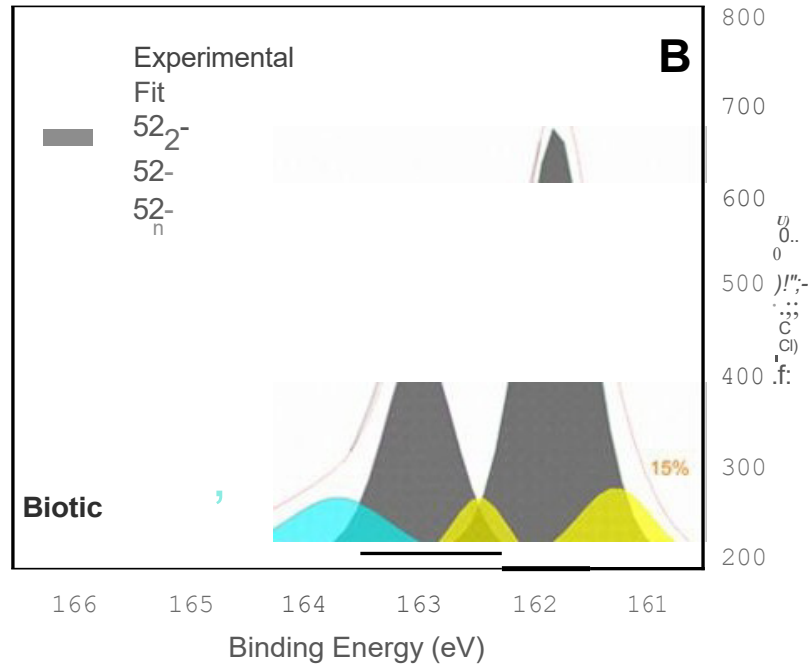
B
Experimental
Fit
15%
Biotic
800
700
600
500
400
300
200
166
165
164
163
162
161
Binding Energy (eV)

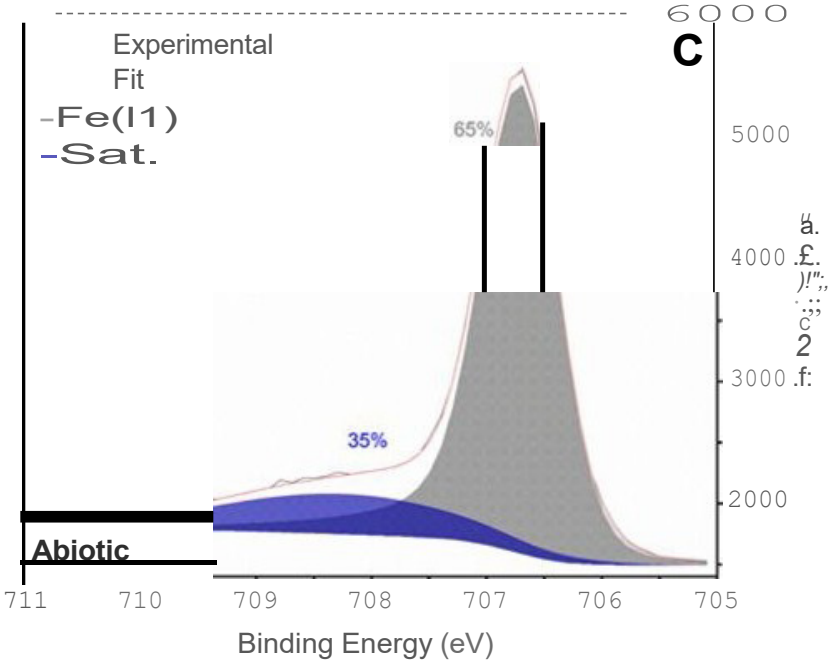
C
Experimental
Fit
-Fe(I1)
-Sat.
65%
35%
Abiotic
6000
5000
4000
3000
2000
711
710
709
708
707
706
705
Binding Energy (eV)

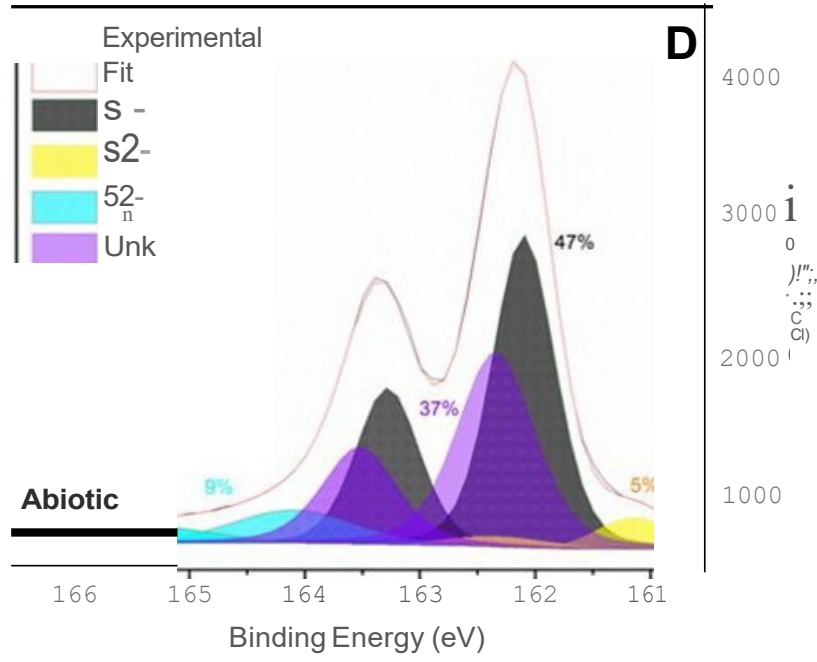
D
Experimental
Fit
Unk
47%
37%
9%
5%
Abiotic
4000
3000
2000
1000
166
165
164
163
162
161
Binding Energy (eV)

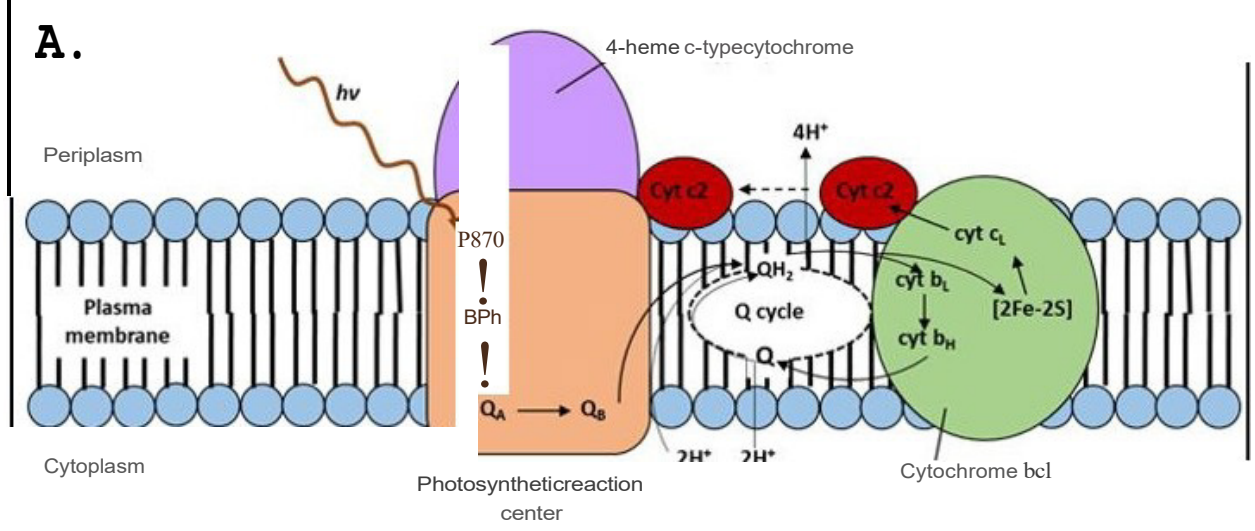
A.
hv
4-heme c-typecytochrome
Periplasm
4H+
Cyt c2
Cyt c2
P870
BPh
Plasma membrane
QH2
Q cycle
Q
cyt cL
cyt bL
cyt bH
[2Fe-2S]
QA
QB
2H+
2H+
Cytoplasm
Photosyntheticreaction center
Cytochrome bcl

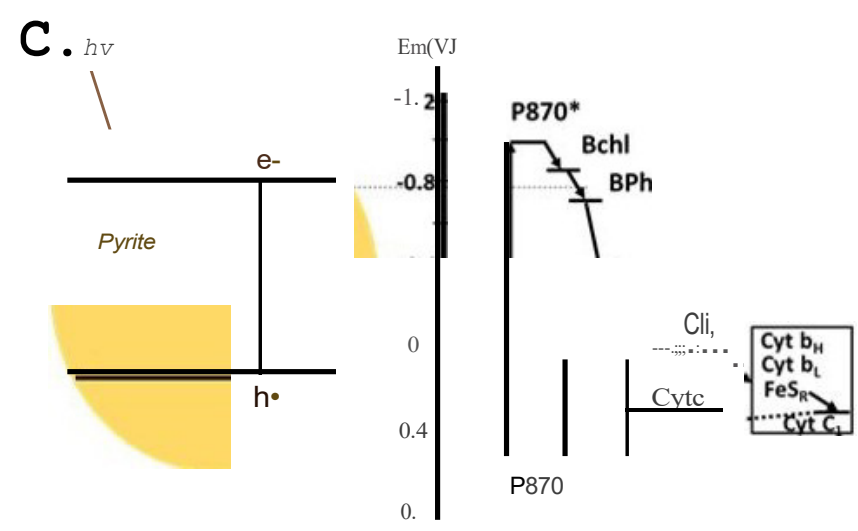
C.
hv
Em(VJ
e-
Pyrite
h•
-1.2
-0.8
0
0.4
0.
P870*
Bchl
BPh
Cli,
Cytc
Cyt bH
Cyt bL
FeSR
Cyt C1
P870

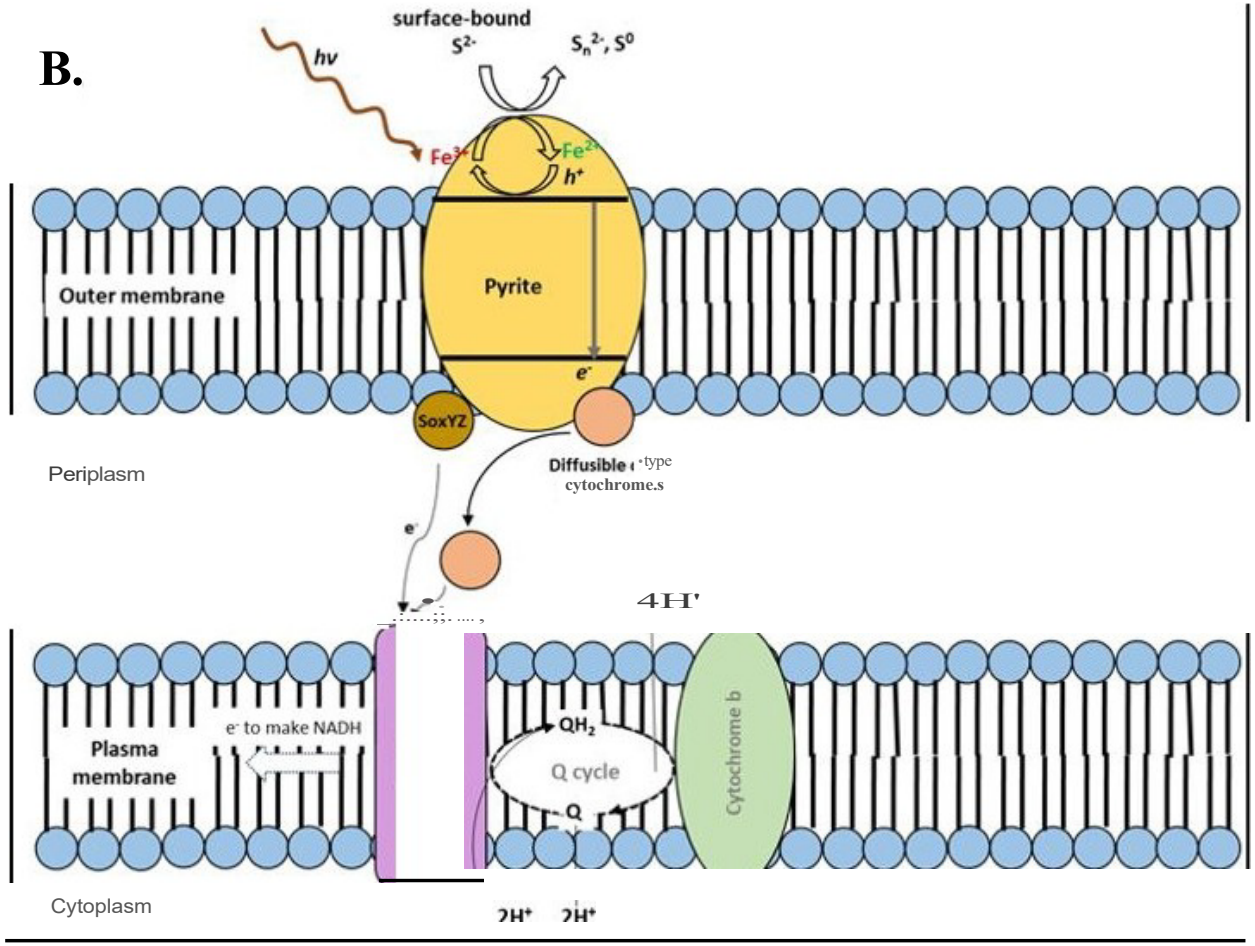
B.
surface-bound
S2-
Sn2-, S0
hv
Fe3+
Fe2+
h+
Outer membrane
Pyrite
e-
SoxYZ
Periplasm
Diffusible
cytochrome.s
e-
4H+
Plasma membrane
e- to make NADH
QH2
Q cycle
Q
Cytochrome b
Cytoplasm
2H+
2H+